SECURITY INFORMATION

NACA RM L52A21

FOR REFERENCE

NOT TO BE TAKEN FROM THIS ROOM

RESEARCH MEMORANDUM

THE AERODYNAMIC CHARACTERISTICS OF A SUPERSONIC AIRCRAFT CONFIGURATION WITH A 40° SWEPTBACK WING THROUGH A MACH NUMBER RANGE FROM 0 TO 2.4 AS OBTAINED FROM VARIOUS SOURCES

By M. Leroy Spearman and Ross B. Robinson

Langley Aeronautical Laboratory
Langley Field, Va.

To UNCLASSIFIED

NACA Restricted Memo dated June 24, 1958

By authority of ARN-128 Date Amt 9-9-58

CLASSIFIED DOCUMENT

This material contains information affecting the National Defense of the United States within the meaning of the espionage laws, Title 18, U.S.C., Secs. 793 and 794, the transmission or revelation of which in any manner to unauthorized person is prohibited by law.

NATIONAL ADVISORY COMMITTEE
FOR AERONAUTICS

WASHINGTON

April 11, 1952

NASA Technical Library
3 1176 01437 0622

~~CONFIDENTIAL~~ Classified Summary
NACA RM L52A21

NATIONAL ADVISORY COMMITTEE FOR AERONAUTICS

RESEARCH MEMORANDUM

THE AERODYNAMIC CHARACTERISTICS OF A SUPERSONIC AIRCRAFT CONFIGURATION WITH A 40° SWEPTBACK WING THROUGH A MACH NUMBER RANGE FROM 0 TO 2.4 AS OBTAINED FROM VARIOUS SOURCES

By M. Leroy Spearman and Ross B. Robinson

SUMMARY

A summary and analysis of results of various investigations concerned with the aerodynamic characteristics of a supersonic aircraft configuration through a Mach number range from 0 to 2.4 have been made. The configuration had a wing with 40° sweepback at the quarter-chord line, aspect ratio 4, taper ratio 0.5, and 10-percent-thick circular-arc sections normal to the quarter-chord line.

The results presented include the static longitudinal and lateral stability characteristics, the aileron characteristics, and the damping-in-roll characteristics. First-order estimates were made of some of the results and these estimates are compared with the experimental results.

INTRODUCTION

During recent years the National Advisory Committee for Aeronautics has been engaged in a series of investigations concerned with the aerodynamic characteristics of a supersonic aircraft configuration having a wing with 40° sweepback at the quarter-chord line, aspect ratio 4, taper ratio 0.5, and 10-percent-thick circular-arc sections normal to the quarter-chord line. Various phases of the investigations covering the subsonic-, transonic-, and supersonic-speed range from a Mach number of 0.16 to a Mach number of 2.32 have been performed by using many test facilities and test techniques (references 1 to 25).

~~CONFIDENTIAL~~

Such an extent of experimental data for one configuration provides an opportunity for determining the variation of its aerodynamic characteristics through the Mach number range. A fundamental purpose of the present paper is to bring together the results of the various investigations and to show comparisons of some of the results with first-order estimates.

Pressure-distribution studies made of the model in the Langley 4- by 4-foot supersonic tunnel at Mach numbers of 1.40 and 1.59 (references 21 to 25), although not included in the present paper, may be useful in interpreting some of the aerodynamic characteristics of the model.

Inasmuch as the model is similar to several flying and proposed aircraft, a comparison of the first-order estimates with the experimental results may be useful in estimating the characteristics of similar configurations.

SYMBOLS

The results of the analysis are referred to the stability axis system (fig. 1) with the reference centers of gravity as indicated in table I.

The coefficients and symbols are defined as follows:

C_L	lift coefficient (Lift/qS where Lift = -Z)
C_D	drag coefficient (Drag/qS where Drag = -X)
C_Y	lateral-force coefficient (Y/qS)
C_l	rolling-moment coefficient (L/qSb)
C_m	pitching-moment coefficient ($M'/qS\bar{c}$)
C_n	yawing-moment coefficient (N/qSb)
C_{h_α}	aileron hinge-moment coefficient $\left(H_a/2M_a q\right)$
X	force along X-axis
Y	force along Y-axis
Z	force along Z-axis

[redacted]

L	moment about X-axis
M'	moment about Y-axis
N	moment about Z-axis
H_a	aileron hinge moment
M_a	moment area of aileron about hinge line
q	free-stream dynamic pressure
b	wing span
S	wing area
$\bar{c}$	wing mean aerodynamic chord $\left(\frac{2}{S}\int_0^{b/2} c^2 dy\right)$
c	airfoil section chord
y	distance along wing span
M	Mach number
V	airspeed
R	Reynolds number based on $\bar{c}$
α	angle of attack of fuselage center line, degrees
ψ	angle of yaw, degrees
i_t	stabilizer incidence angle with respect to fuselage center line, degrees
δ_a	aileron deflection in free-stream direction, degrees
ϵ	effective angle of downwash, degrees
t	ratio of aileron trailing-edge thickness to hinge-line thickness
L/D	lift-drag ratio $\left(C_L/C_D\right)$
C_{L_α}	lift-curve slope $\left(\partial C_L/\partial\alpha\right)$

[redacted]

$\partial C_m/\partial i_t$ stabilizer effectiveness, rate of change of pitching-moment coefficient with stabilizer incidence angle

$\partial \epsilon/\partial \alpha$ downwash factor, rate of change of effective downwash angle with angle of attack

n_o tail-off aerodynamic-center location, percent $\bar{c}$

n_p neutral-point location, percent $\bar{c}$

C_{Y_ψ} lateral-force derivative, rate of change of lateral-force coefficient with angle of yaw $\left(\partial C_Y/\partial \psi\right)$

C_{n_ψ} directional-stability derivative, rate of change of yawing-moment coefficient with angle of yaw $\left(\partial C_n/\partial \psi\right)$

C_{l_ψ} effective-dihedral derivative, rate of change of rolling-moment coefficient with angle of yaw $\left(\partial C_l/\partial \psi\right)$

$C_{l_{\psi_{C_L}}}$ rate of change of effective-dihedral with lift coefficient, $\frac{\partial}{\partial C_L}\left(\frac{\partial C_l}{\partial \psi}\right)$

$C_{l_{\delta_a}}$ rate of change of rolling-moment coefficient with aileron deflection $\left(\partial C_l/\partial \delta_a\right)$

C_{l_p} damping-in-roll factor, rate of change of rolling-moment coefficient with rolling velocity $\left(\partial C_l/\partial \frac{pb}{2V}\right)$

$pb/2V$ wing-tip helix angle, radians $\left(C_l/C_{l_p}\right)$

p rolling velocity, radians per second

C_{h_α} rate of change of aileron hinge-moment coefficient with angle of attack $\left(\partial C_{h_\alpha}/\partial \alpha\right)$

C_{h_δ} rate of change of aileron hinge-moment coefficient with aileron deflection $\left(\partial C_{h_\alpha}/\partial \delta_a\right)$

[redacted]

MODELS AND APPARATUS

Although some minor differences in the various models were present, the complete model shown in figures 2 and 3(a) is representative of the models investigated in the Langley 300 MPH 7- by 10-foot tunnel ("small fuselage model," reference 1) the Langley 9-inch supersonic tunnel (model 2, reference 10) the Langley 4- by 4-foot supersonic tunnel, and in one rocket model flight. The wing-flow model was the same except that only a half-model or semispan model was used (fig. 3(b)).

The investigations conducted by the transonic-bump method, the wall reflection-plane method, and in the Langley 9- by 12-inch supersonic blowdown tunnel were made by using semispan wing-body models in which the wing plan form was the same as for the basic model although there were some differences in the body shape and wing location. These models are shown in figures 3(c), 3(d), and 3(e).

The rocket-model investigation concerned only with aileron characteristics utilized an RM-5 rocket model equipped with three fins similar to the wing of the basic model (fig. 3(f)).

Static forces and moments on restrained models were recorded in all investigations with the exception of the wing-flow tests and rocket-model tests. The wing-flow tests and complete-model rocket test made use of the oscillating-model technique; whereas the aileron tests with the RM-5 rocket made use of the free-rolling model technique. Complete details of the models, test techniques, test conditions, and accuracy of results may be found in the reference reports.

RESULTS AND DISCUSSION

A summary of the various sources of experimental results giving the Mach number and Reynolds number range of each, the model center-of-gravity location, the configuration tested, the reference numbers and figure number in which the data from these sources may be found, is presented in table I.

When the results from the various sources are compared it should be kept in mind that there are slight geometric differences between some of the models as well as variations in test conditions, accuracy, and model flexibility. Discrepancies in results that arise as a consequence of model differences and differences due to center-of-gravity location are, in some cases, apparent although the effects of differences in wing location and body shape have not been determined.

[redacted]

Since results were not available throughout the Mach number range for all of the parameters, some estimated variations of the parameters with Mach number have been included. Although no attempt has been made to fair the experimental results, some faired curves based on the experimental and the estimated results are presented as possible variations of the various parameters with Mach number. In some cases, the curves have been extrapolated into regions where no data are available.

Lift and Drag Characteristics

The experimental lift and drag characteristics are presented in figures 4 to 7 and faired curves summarizing the results are presented in figure 8.

Lift.- The variation of lift coefficient C_L with Mach number for various angles of attack is shown in figure 4. It is difficult to establish any trends from the wing-flow results in the transonic range because of the differences between the two curves. These differences are generally within the accuracy of the wing-flow technique. The notations, run 1 and run 2, are used to identify the results of two test dives for slightly different Reynolds number ranges (see table I). The bump model was constructed symmetrically and the lift values for this model were corrected for the angle-of-attack difference by adding to the bump values the lift coefficient for $\alpha = 0^\circ$ for the complete model at $M = 0.16$. Results from the rocket-model test are shown by the flagged symbols at $\alpha = -4^\circ$, -2°, and 0°.

The lift summary (fig. 8) indicates that in the subsonic range the lift variations with Mach number for constant angles of attack gradually diverge and then converge in the supersonic range. The shaded area in the transonic range indicates a region of estimated uncertainty with regard to the variation of C_L with M.

Lift-curve slope.- The variation of the lift-curve slope, C_{L_α}, with Mach number is shown in figure 5. The theoretical variation of C_{L_α} shown in the subsonic range was obtained by the use of reference 26 and represents a compressibility correction for wing alone applied to the low-speed complete-model experimental results. The theoretical variation in the supersonic range is for the wing alone and was determined by the method of reference 27.

It is difficult to reach any conclusions concerning the lift-curve slopes in the transonic range since the large differences in the results from the various facilities mask the effects of Mach number, Reynolds number, and nonlinear lift variations with angle of attack.

With the exception of the low-speed results and the results from the Langley 9-inch supersonic tunnel, all the data presented in figure 5 apply to the model with the thickened trailing-edge aileron ($t = 0.5$). The effect of the thickened trailing edge at low speeds is not known. Transonic-bump results presented in reference 15 show lift-curve slopes for the basic circular-arc wing that are about 15 percent lower than those for the thickened-profile wing. Wing-flow tests, however, indicated no difference between the basic-wing lift-curve slope and that for the thickened-profile wing. Results of the tests in the Langley 4- by 4-foot tunnel (reference 20) indicate a slightly higher C_{L_α} for the thickened profile whereas the tests in the Langley 9- by 12-inch tunnel (reference 19) indicated no difference between the lift-curve slopes for the two profiles.

The variation of C_{L_α} with Mach number (fig. 8) was guided, in part, by the results of reference 28 which indicates that, for 35° and 45° swept wings, the lift-curve slope increases smoothly through the transonic range to a maximum at a Mach number of about 0.9 and then decreases smoothly. The shaded area in the transonic region represents a region of uncertainty in the lift-curve slope.

Drag.- The variation of drag coefficient C_D with Mach number for various lift coefficients is shown in figure 6. The symbols at $M = 0.607$ and 0.934 were obtained from a faired curve of C_D against C_L presented in reference 14. The dashed line is indicative of the type of variation of C_D with Mach number near zero lift as shown by reference 14. The solid line was obtained from a rocket-model flight near zero lift. Agreement of the rocket-model results with those from the wall model below the drag rise is coincidental inasmuch as the wall model did not have a tail and, as a result, should have less drag than the rocket model. As pointed out in reference 28, however, the wing-fuselage drag at zero lift obtained with this wall model is not considered reliable.

It is interesting to note that the drag obtained at the highest Mach number for the rocket model ($M = 1.36$) is in good agreement with the complete-model drag obtained in the Langley 4- by 4-foot supersonic tunnel ($M = 1.40$) despite the large difference in the Reynolds number.

Sufficient drag data were available so that the drag for zero lift (fig. 8) may be regarded as having a reasonable degree of certainty. The variation of drag coefficient with Mach number indicates a rather sharp drag rise through the transonic range beginning at $M \approx 0.9$, with a peak drag at $M \approx 1.1$. In the transonic region, the variation of the zero-lift drag curve was used as a guide in fairing the drag curves for lift coefficients other than zero.

[redacted]

Lift-drag ratio.- The variation of the lift-drag ratio L/D with Mach number (fig. 7) was obtained from figure 6 for the tunnel tests of the complete model and the wall tests of the wing-fuselage model. No L/D ratios for the complete model were obtained in the transonic range since drag results were not available for the complete model in this range except for the rocket tests near zero lift.

As might be expected, the lift-drag ratios shown in figure 8 remain about constant up to the Mach number for the drag rise and then decrease through the transonic range in a manner largely due to the drag increase. In the supersonic range the lift-drag ratios are quite low although a slight increase in L/D with increasing Mach number is indicated. The lift-drag ratios shown for $C_L = 0.3$ are essentially the maximum L/D ratios obtainable. The low lift-drag ratios at supersonic speeds are about what would be expected as indicated by the results of references 23 and 24 wherein the L/D ratios for the wing alone at $M = 1.59$ and 1.40 were calculated by means of linear theory and compared with experimental wing-body results.

Longitudinal Stability Characteristics

The experimental longitudinal stability characteristics are presented in figures 9 to 12 and are summarized in figure 13.

Stabilizer effectiveness.- The variation of the stabilizer effectiveness $\partial C_m/\partial i_t$ with Mach number is presented in figure 9. The theoretical variation with Mach number is that due only to the change in the horizontal-tail lift-curve slope.

The subsonic variation is based on the experimental results at $M = 0.16$ and the supersonic variation is based on the experimental results at $M = 1.40$. The tail lift-curve slope was assumed to be the same as that for the wing inasmuch as their plan forms are similar.

As a result the variation of stabilizer effectiveness $\partial C_m/\partial i_t$ with Mach number (fig. 13) is similar to that shown for C_{L_α} of the wing. Because of the decreased stabilizer lift-curve slope, the stabilizer effectiveness at supersonic speeds is considerably less than its low-speed value. The shaded area in the transonic range indicates a region of uncertainty in $\partial C_m/\partial i_t$ as a result of uncertainties in C_{L_α}.

Downwash.- The variation with Mach number of the change of effective downwash angle with angle of attack $\partial\epsilon/\partial\alpha$ (fig. 10) was obtained from tests in the Langley 300 MPH 7- by 10-foot tunnel, tests in the

Langley 4- by 4-foot supersonic tunnel, and wing-flow tests. The low-speed value of $\partial\epsilon/\partial\alpha$ near zero lift was estimated by the method of reference 29. The theoretical values of $\partial\epsilon/\partial\alpha$ at supersonic speeds (obtained from reference 25) account for the downwash of the wing as well as the downwash of the body.

The downwash variation with Mach number (fig. 13) indicates a peak value of $\partial\epsilon/\partial\alpha$ at $M = 0.9$. This type of variation and peak of $\partial\epsilon/\partial\alpha$ was obtained both from the wing-flow tests and from bump tests of a similar model having the same tail height (see reference 30.)

The effective downwash at supersonic speeds (fig. 13) is considerably reduced from its low-speed value.

Tail-off aerodynamic center and neutral point.- The variation of the tail-off aerodynamic-center location n_o with Mach number is shown in figure 11. Irregularity in the location of the aerodynamic center shown by the wing-flow and wall results is similar to that shown in the C_{L_α} variation.

The test in the Langley 9- by 12-inch supersonic blowdown tunnel at $M = 1.90$ was for a model with a slightly different fuselage and wing location; however, the results follow the trend indicated by the results from the Langley 4- by 4-foot supersonic tunnel.

The variation of the neutral-point location n_p (center-of-gravity location for neutral stability for complete model) with Mach number is presented in figure 12. The more forward location of the neutral point indicated by the rocket-model tests at $M = 1.34$ results in part from the high C_{L_α} obtained for the rocket model (see fig. 5).

The tail-off aerodynamic center location and the neutral-point location (fig. 13) shift rearward about 25 percent of the mean aerodynamic chord from subsonic speeds to supersonic speeds. A slight forward shift indicated in the neutral point near $M = 0.9$ may result from the rapid increase in effective downwash at the tail for this Mach number. Aside from the transonic range, both the aerodynamic-center location and the neutral-point location are essentially constant with Mach number. Although the difference between the aerodynamic-center location and the neutral-point location indicates a nearly constant tail contribution throughout the Mach number range, it is evident that this constant tail contribution is a result of compensating changes in $\partial C_m/\partial i_t$ and $\partial\epsilon/\partial\alpha$.

[redacted]

Sideslip Derivatives

The experimental sideslip derivatives are presented in figures 14 to 16 and are summarized in figure 17.

Lateral-force derivative.- The variation of the lateral-force derivative C_{Y_ψ} with Mach number is shown in figure 14. The estimated variation of C_{Y_ψ} with Mach number is that due only to the change in vertical-tail lift-curve slope. The subsonic variation was obtained by applying a compressibility correction obtained from reference 26 to the $M = 0.16$ experimental results. The supersonic variation was based on the $M = 1.40$ experimental results with the vertical-tail lift-curve slope variation with Mach number determined from charts presented in reference 27. A vertical-tail aspect ratio of 1.5 was used in the lift-curve-slope estimates. This aspect ratio is that for the exposed vertical tail with a correction obtained from reference 31 to account for the end-plate effect of the horizontal tail. This end-plate correction has been used at both subsonic and supersonic speeds in the calculation of the theoretical vertical-tail lift-curve slopes. It was assumed that the value of C_{Y_ψ} for the model with the tail off does not change with Mach number. Theoretical and experimental results indicate this assumption is reasonable for a body of revolution (see reference 32) and the results of reference 26 indicate that, for the subsonic range, at least, the variation of C_{Y_ψ} with Mach number for the wing at low lift coefficients would be negligible.

Results from the tests in the Langley 9-inch supersonic tunnel ($M = 1.55$, 1.90, 2.32; reference 10) were converted from the wind axes to the stability axes. The results from the Langley 4- by 4-foot tunnel indicate slightly lower values of C_{Y_ψ} than those obtained from the tests in the Langley 9-inch tunnel. As pointed out in reference 7, some of this difference is a result of a small opening made in the vertical tail of the Langley 4- by 4-foot tunnel model to permit deflection of the horizontal tail. Tests made with the opening sealed (reference 9) indicated that C_{Y_ψ} might be increased about 10 percent.

The transition of C_{Y_ψ} from subsonic speeds to supersonic speeds is faired smoothly (fig. 17) since the low aspect ratio of the vertical tail should result in a smooth variation of tail lift-curve slope through the transonic range. At supersonic speeds, of course, the decrease in C_{Y_ψ} with increasing Mach number is a result of a decreasing vertical-tail lift-curve slope.

Directional-stability derivative.- The variation of the directional-stability derivative C_{n_ψ} with Mach number is presented in figure 15. The estimated variation of C_{n_ψ} with Mach number for the complete model is that due only to the change in the vertical-tail lift-curve slope. Other factors which have been neglected that could affect the variation of C_{n_ψ} with Mach number include changes in the interference effects and a possible shift in the tail center of pressure. The value of C_{n_ψ} for the tail-off case was assumed to be constant with Mach number. This assumption is substantiated for bodies of revolution by the experimental and theoretical results presented in reference 32. Reference 26 indicates that C_{n_ψ} for the wing alone might become slightly less stable at the higher lift coefficients.

With regard to the transonic results it should be remembered that the rocket-model center of gravity is farther forward than that for the tunnel models; hence, the directional stability of the rocket model should be greater. When correction is made for the difference in center-of-gravity location the values of C_{n_ψ} for the rocket model would be reduced approximately 15 percent. The difference between the results from the 4- by 4-foot tunnel and those from the 9-inch tunnel is caused by the differences in C_{Y_ψ} previously discussed.

The variation of C_{n_ψ} as shown in figure 17 is similar to that for C_{Y_ψ} inasmuch as the vertical-tail lift-curve slope is the controlling factor in either case. Of some concern at supersonic speeds is the trend of C_{n_ψ} towards zero, or directional instability, for the complete model. If the tail-off value of C_{n_ψ} remains the same while the vertical-tail lift-curve slope continues to decrease with Mach number, the unstable moment of the wing-body combination may eventually outweigh the stable contribution of the tail.

Effective dihedral derivative.- The variation of the rolling-moment-due-to-yaw or effective dihedral derivative C_{l_ψ} near $C_L = 0$ and the variation of effective dihedral with lift coefficient $C_{l_\psi C_L}$ with Mach number are shown in figure 16 for the complete model and for the model with the tail off. Experimental results were available only from the 300 MPH 7- by 10-foot tunnel tests and the 4- by 4-foot tunnel tests.

[redacted]

The estimated variation of C_{l_ψ} with Mach number for the complete model is that due only to the change in the vertical-tail lift-curve slope. The variation of $C_{l_{\psi_{C_L}}}$ with Mach number in the subsonic range for the model with the tail off was determined by applying a compressibility correction obtained from reference 26 to the low-speed experimental value. Simple estimates of the vertical-tail contribution to $C_{l_{\psi_{C_L}}}$ indicate no variation with Mach number in the subsonic range.

A large effect of the vertical tail on C_{l_ψ} at $C_L \approx 0.1$ is evidenced by figure 17 in that almost all the rolling-moment due to yaw is produced by the vertical tail. Opposite to the usual low-speed result, the effective dihedral of the wing-body combination becomes negative through part of the supersonic range. It is indicated in reference 33 that the effective dihedral for sweptback wings at positive lifts is positive as long as the wing leading edge is subsonic. At higher Mach numbers the effective dihedral reduces towards zero.

The trends indicated by C_{Y_ψ}, C_{n_ψ}, and C_{l_ψ} in the subsonic range are similar to the trends shown in reference 34 for a straight-wing model in the Mach number range from 0.40 to 0.88.

Aileron Characteristics

The experimental aileron characteristics are presented in figures 18 and 19 and are summarized in figure 20.

Aileron effectiveness.- The aileron effectiveness $C_{l_{\delta_a}}$ for small deflections against Mach number (fig. 18) was obtained for two aileron profiles: the basic circular-arc aileron and the flat-sided aileron having a ratio of trailing-edge thickness to hinge-line thickness of 0.5.

The low-speed value of $C_{l_{\delta_a}}$ was estimated by the use of reference 35 and the theoretical values of $C_{l_{\delta_a}}$ at $M = 1.40$ and 1.59 were obtained from reference 20. Although the theoretical values of $C_{l_{\delta_a}}$ are somewhat higher than the experimental values, the effects of trailing-edge angle are the same.

The variation of aileron effectiveness with Mach number as summarized in figure 20 indicates the rapid decrease in $C_{l_{\delta_a}}$ in the transonic range and the reversal in effectiveness of the circular-arc profile. It should be pointed out, however, that these results are for a rigid wing and are for small aileron deflections near zero lift and that above about 4° deflection the effectiveness is positive. Thickening the trailing edge eliminated the reversal shown by the circular-arc profile and increased the effectiveness.

Aileron hinge moments.- The variation of the aileron hinge-moment characteristics C_{h_α} and $C_{h_{\delta_a}}$ with Mach number is presented in figure 19. Low-speed values were estimated by the use of reference 36.

The variation of C_{h_α} and $C_{h_{\delta_a}}$ with Mach number (fig. 20) in the subsonic range is in accordance with the trends indicated in reference 37. It is pointed out in reference 37 that, when the trailing-edge angle is small (corresponding to $t = 0.5$), the values of C_{h_α} and $C_{h_{\delta_a}}$ usually increase in absolute magnitude as the Mach number is increased; whereas, when the trailing-edge angle is large (circular-arc) the values of C_{h_α} and $C_{h_{\delta_a}}$ of smooth low-drag airfoils almost invariably become more positive. It is not possible, of course, to attribute all the variation in C_{h_α} and $C_{h_{\delta_a}}$ to changes in Mach number as a large part of the variation may result from changes in the boundary-layer transition point caused by changes in the Reynolds number as the Mach number is increased. Since it might be expected that the aileron hinge moments would be especially sensitive to Reynolds number changes, the correlation of hinge-moment results from the various sources should be used with caution.

Rolling Characteristics

The basic rolling characteristics of the model for both the circular-arc and the $t = 0.5$ aileron are presented in figures 21 and 22 and are summarized in figure 23.

Damping-in-roll derivative.- The variation of the damping-in-roll derivative C_{l_p} with Mach number is presented in figure 21. The only available experimental data were those obtained at transonic speeds by using the transonic bump and at $M = 1.90$ in the Langley 9- by 12-inch supersonic tunnel. These results (reference 15) were obtained by the twisted-wing method.

The low-speed value of C_{l_p} was obtained by the method of reference 38 and the variation of C_{l_p} with Mach number at subsonic speeds was determined by the use of reference 26. In the Mach number range from 1.15 to 1.36 the theoretical values of C_{l_p} were obtained by the use of reference 39. The theoretical values of C_{l_p} in the Mach number range from 1.40 to 1.90 were obtained from reference 27. The theoretical values of C_{l_p} are all for the wing alone.

The variation of C_{l_p} with Mach number in the transonic region (figs. 21 and 23) is indicated to be somewhat different for the wings with the two profiles. It is pointed out in reference 15 that these differences are probably a result of differences in the lift-curve slope for the two wings and differences in the type of separation near the trailing edge.

Rolling effectiveness.- The variation of the rolling effectiveness per degree of aileron deflection $\frac{pb}{2V}\Big/\delta_a$ with Mach number is presented in figure 22. Values for the rocket model in the transonic range were determined directly from the flight of rolling models. The bump values in the transonic range were determined by use of the experimental $C_{l_{\delta_a}}$ and C_{l_p} values from figures 18 and 21. Tunnel values were computed from the experimental values of $C_{l_{\delta_a}}$ and the theoretical values of C_{l_p} except for the flagged point at $M = 1.90$ which was determined from experimental values of both $C_{l_{\delta_a}}$ and C_{l_p}.

The reversal of roll (figs. 22 and 23) indicated in the transonic range for the wing having the circular-arc profile aileron is a result of the reversal in $C_{l_{\delta_a}}$ already discussed. This reversal, as shown in references 12 and 14, should disappear for deflections above about 4°.

CONCLUSIONS

An analysis of the results of various investigations concerned with the aerodynamic characteristics of a swept-wing supersonic aircraft configuration through a Mach number range from 0 to 2.4 indicated the following conclusions:

[redacted]

1. In the transonic region, the differences in the lift and lift-curve slopes obtained from the various facilities were such that Mach number or Reynolds number effects could not be evaluated.

2. A relatively sharp drag rise began near $M = 0.9$ with a peak drag at $M = 1.1$. The maximum lift-drag ratio at supersonic speeds was about 3.5 and was in fair agreement with the theoretically predicted value.

3. An increase in the static margin occurred through the transonic range largely as a result of an increase in the longitudinal stability of the wing-fuselage combination. A constant tail contribution to the longitudinal stability was indicated throughout the Mach number range although the factors comprising the tail contribution varied widely.

4. The side force due to yaw and the directional stability increased smoothly at subsonic speeds with increasing speed and decreased smoothly at supersonic speeds in a manner mainly due to the variation of the vertical-tail lift-curve slope. A trend towards directional instability was indicated for higher Mach numbers.

5. Unlike the low-speed effect, the variation of effective dihedral with lift coefficient in the low supersonic range was quite small, and there was an indication of reversal of effective dihedral from positive to negative for the model with the tail off.

6. The effectiveness of the aileron in producing roll was much less at supersonic speeds than at subsonic speeds with the loss of effectiveness being somewhat greater than that indicated by theory. The effectiveness of a circular-arc contour aileron reversed in the transonic range for aileron deflections of less than 4°. Thickening the trailing edge of the aileron resulted in an elimination of the reversal and increased the rolling effectiveness as well as the hinge moments throughout the Mach number range. Similar effects of trailing-edge thickness on the rolling effectiveness and the hinge moments were indicated by theory.

Langley Aeronautical Laboratory
National Advisory Committee for Aeronautics
Langley Field, Va.

[redacted]

REFERENCES

1. Weil, Joseph, Comisarow, Paul, and Goodson, Kenneth W.: Longitudinal Stability and Control Characteristics of an Airplane Model Having a 42.8° Sweptback Circular-Arc Wing with Aspect Ratio 4.00, Taper Ratio 0.50, and Sweptback Tail Surfaces. NACA RM L7G28, 1947.

2. Goodson, Kenneth W., and Comisarow, Paul: Lateral Stability and Control Characteristics of an Airplane Model Having a 42.8° Sweptback Circular-Arc Wing with Aspect Ratio 4.00, Taper Ratio 0.50, and Sweptback Tail Surfaces. NACA RM L7G31, 1947.

3. Crane, Harold L., and Adams, James J.: Wing-Flow Measurements of Longitudinal Stability and Control Characteristics of a Supersonic Airplane Configuration Having a 42.8° Sweptback Circular-Arc Wing with Aspect Ratio 4.0, Taper Ratio 0.50, and Sweptback Tail Surfaces. NACA RM L50B09, 1950.

4. D'Aiutolo, Charles T., and Mason, Homer P.: Preliminary Results of the Flight Investigation between Mach Numbers of 0.80 and 1.36 of a Rocket-Powered Model of a Supersonic Airplane Configuration Having a Tapered Wing with Circular-Arc Sections and 40° Sweepback. NACA RM L50H29a, 1950.

5. Spearman, M. Leroy: An Investigation of a Supersonic Aircraft Configuration Having a Tapered Wing with Circular-Arc Sections and 40° Sweepback. Static Longitudinal Stability and Control Characteristics at a Mach Number of 1.40. NACA RM L9L08, 1950.

6. Spearman, M. Leroy, and Hilton, John H., Jr.: An Investigation of a Supersonic Aircraft Configuration Having a Tapered Wing with Circular-Arc Sections and 40° Sweepback. Static Longitudinal Stability and Control Characteristics at a Mach Number of 1.59. NACA RM L50E12, 1950.

7. Spearman, M. Leroy: An Investigation of a Supersonic Aircraft Configuration Having a Tapered Wing with Circular-Arc Sections and 40° Sweepback. Static Lateral Stability Characteristics at Mach Numbers of 1.40 and 1.59. NACA RM L50C17, 1950.

8. Robinson, Ross B.: An Investigation of a Supersonic Aircraft Configuration Having a Tapered Wing with Circular-Arc Sections and 40° Sweepback. Static Lateral Control Characteristics at Mach Numbers of 1.40 and 1.59. NACA RM L50I11, 1950.

[redacted]

9. Smith, Norman F., and Marte, Jack E.: An Investigation of a Supersonic Aircraft Configuration Having a Tapered Wing with Circular-Arc Sections and 40° Sweepback. Force Characteristics of a Complete Configuration and its Various Components at Mach Numbers of 1.40 and 1.59. NACA RM L50K14, 1951.

10. Ellis, Macon C., Jr., Hasel, Lowell E., and Grigsby, Carl E.: Supersonic-Tunnel Tests of Two Supersonic Airplane Model Configurations. NACA RM L7J15, 1947.

11. Sandahl, Carl A.: Free-Flight Investigation at Transonic and Supersonic Speeds of the Rolling Effectiveness of a 42.7° Sweptback Wing Having Partial-Span Ailerons. NACA RM L8E25, 1948.

12. Sandahl, Carl A.: Free-Flight Investigations at Transonic and Supersonic Speeds of the Rolling Effectiveness of Several Aileron Configurations on a Tapered Wing Having 42.7° Sweepback. NACA RM L8K23, 1949.

13. Turner, Thomas R., Lockwood, Vernard E., and Vogler, Raymond D.: Preliminary Investigation of Various Ailerons on a 42° Sweptback Wing for Lateral Control at Transonic Speeds. NACA RM L8D21, 1948.

14. Turner, Thomas R., Lockwood, Vernard E., and Vogler, Raymond D.: Aerodynamic Characteristics at Subsonic and Transonic Speeds of a 42.7° Sweptback Wing Model Having an Aileron with Finite Trailing-Edge Thickness. NACA RM L8K02, 1949.

15. Lockwood, Vernard E.: Damping-in-Roll Characteristics of a 42.7° Sweptback Wing as Determined from a Wind-Tunnel Investigation of a Twisted Semispan Wing. NACA RM L9F15, 1949.

16. Thompson, Robert F.: Investigation of a 42.7° Sweptback Wing Model to Determine the Effects of Trailing-Edge Thickness on the Aileron Hinge-Moment and Flutter Characteristics at Transonic Speeds. NACA RM L50J06, 1950.

17. Sivells, James C., and Conner, D. William: Preliminary Investigation at a Mach Number of 1.9 and a Reynolds Number of 2,200,000 of Three Ailerons Applicable to the Bell XS-2 Airplane Design. NACA RM L8D02, 1948.

18. Sivells, James C., and Goin, Kennith L.: Experimental and Calculated Hinge Moments of Two Ailerons on a 42.7° Sweptback Wing at a Mach Number of 1.9. NACA RM L8K24a, 1949.

[redacted]

19. Goin, Kennith L.: Investigation at a Mach Number of 1.9 and a Reynolds Number of 2.2 × 10^6 of Several Flap-Type Lateral-Control Devices on a Wing Having 42.7° Sweepback of the Leading Edge. NACA RM L9A18a, 1949.

20. Spearman, M. Leroy, and Webster, Robert A.: An Investigation at Mach Numbers of 1.40 and 1.59 of the Effects of Aileron Profile on the Aerodynamic Characteristics of a Complete Model of a Supersonic Aircraft Configuration. NACA RM L50J31, 1951.

21. Cooper, Morton, Smith, Norman F., and Kainer, Julian H.: A Pressure-Distribution Investigation of a Supersonic Aircraft Fuselage and Calibration of the Mach Number 1.59 Nozzle of the Langley 4- by 4-Foot Supersonic Tunnel. NACA RM L9E27a, 1949.

22. Hasel, Lowell E., and Sinclair, Archibald R.: A Pressure-Distribution Investigation of a Supersonic-Aircraft Fuselage and Calibration of the Mach Number 1.40 Nozzle of the Langley 4- by 4-Foot Supersonic Tunnel. NACA RM L50B14a, 1950.

23. Cooper, Morton, and Spearman, M. Leroy: An Investigation of a Supersonic Aircraft Configuration Having a Tapered Wing with Circular-Arc Sections and 40° Sweepback. A Pressure-Distribution Study of the Aerodynamic Characteristics of the Wing at Mach Number 1.59. NACA RM L50C24, 1950.

24. Smith, Norman F., Kainer, Julian H., and Webster, Robert A.: An Investigation of a Supersonic Aircraft Configuration Having a Tapered Wing with Circular-Arc Sections and 40° Sweepback. A Pressure-Distribution Study of the Aerodynamic Characteristics of the Wing at Mach Number 1.40. NACA RM L51C06, 1951.

25. Grant, Frederick C., and Gapcynski, John P.: An Investigation of a Supersonic Aircraft Configuration Having a Tapered Wing with Circular-Arc Sections and 40° Sweepback. Estimated Downwash Angles Derived from Pressure Measurements on the Tail at Mach Numbers of 1.40 and 1.59. NACA RM L51L17, 1952.

26. Fisher, Lewis R.: Approximate Corrections for the Effects of Compressibility on the Subsonic Stability Derivatives of Swept Wings. NACA TN 1854, 1949.

27. Harmon, Sidney M., and Jeffreys, Isabella: Theoretical Lift and Damping in Roll of Thin Wings with Arbitrary Sweep and Taper at Supersonic Speeds. Supersonic Leading and Trailing Edges. NACA TN 2114, 1950.

[redacted]

28. Donlan, Charles J., Myers, Boyd C., II, and Mattson, Axel T.: A Comparison of the Aerodynamic Characteristics at Transonic Speeds of Four Wing-Fuselage Configurations as Determined from Different Test Techniques. NACA RM L50H02, 1950.

29. Purser, Paul E., Spearman, M. Leroy, and Bates, William R.: Preliminary Investigation at Low Speed of Downwash Characteristics of Small-Scale Sweptback Wings. NACA TN 1378, 1947.

30. Sleeman, William C., Jr., and Becht, Robert E.: Aerodynamic Characteristics of a Wing with Quarter-Chord Line Swept Back 35°, Aspect Ratio 4, Taper Ratio 0.6, and NACA 65A006 Airfoil Section. Transonic-Bump Method. NACA RM L9B25, 1949.

31. Murray, Harry E.: Wind-Tunnel Investigation of End-Plate Effects of Horizontal Tails on a Vertical Tail Compared with Available Theory. NACA TN 1050, 1946.

32. Allen, H. Julian: Estimation of the Forces and Moments Acting on Inclined Bodies of Revolution of High Fineness Ratio. NACA RM A9I26, 1949.

33. Jones, Arthur L., Spreiter, John R., and Alksne, Alberta: The Rolling Moment Due to Sideslip of Triangular, Trapezoidal, and Related Plan Forms in Supersonic Flow. NACA TN 1700, 1948.

34. Kuhn, Richard E., and Wiggins, James W.: Static Lateral Stability Characteristics of a $\frac{1}{10}$ - Scale Model of the X-1 Airplane at High Subsonic Mach Numbers. NACA RM L51F01a, 1951.

35. Lowry, John G., and Schneiter, Leslie E.: Estimation of Effectiveness of Flap-Type Controls on Sweptback Wings. NACA TN 1674, 1948.

36. Toll, Thomas A., and Schneiter, Leslie E.: Approximate Relations for Hinge-Moment Parameters of Control Surfaces on Swept Wings at Low Mach Numbers. NACA TN 1711, 1948.

37. Langley Research Staff (Compiled by Thomas A. Toll): Summary of Lateral-Control Research. NACA Rep. 868, 1947. (Formerly NACA TN 1245.)

38. Polhamus, Edward C.: A Simple Method of Estimating the Subsonic Lift and Damping in Roll of Sweptback Wings. NACA TN 1862, 1949.

[redacted]

39. Malvestuto, Frank S., Jr., Margolis, Kenneth, and Ribner, Herbert S.: Theoretical Lift and Damping in Roll at Supersonic Speeds of Thin Sweptback Tapered Wings with Streamwise Tips, Subsonic Leading Edges, and Supersonic Trailing Edges. NACA Rep. 970, 1950. (Formerly NACA TN 1860.)

[redacted]

TABLE I.- SUMMARY OF TEST FACILITIES AND RESULTS

Source	M	R	c.g. (percent $\bar{c}$)	Configuration	Reference	Figure
Langley 300 MPH 7- by 10-foot tunnel	0.16	2,150,000	26	Complete model and components	1 2	4 to 7, 9 to 12, 14 to 16, 18
Wing-flow	0.55 to 1.10	360,000 to 840,000	23	Complete semispan model	3	4, 5, 9, 10 to 12
Rocket model	0.80 to 1.36	5,600,000 to 11,050,000	10.9	Complete model	4	4 to 6, 12 and 15
Langley 4- by 4-foot supersonic tunnel	1.40 and 1.59	600,000 and 575,000	25	Complete model and components	5, 6 7, 8 20	4 to 7, 9 to 12, 14 to 16, 18 and 19
Langley 9-inch supersonic tunnel	1.55, 1.90, and 2.32	410,000, 370,000, and 310,000	25	Complete model	10	4 to 7, 12, 14 and 15
Transonic bump	0.5 to 1.15	820,000 to 1,220,000	18.3	Wing-body combination	14 15 16	4, 5, 15, 18 19 and 21
Wall model	0.43 to 0.94	750,000 to 1,118,000	18.3	Wing-body combination	14	6, 7 and 11
Langley 9- by 12-inch supersonic blowdown tunnel	1.9	2,200,000	25	Wing alone and wing-body combination	19 15 18	11, 15, 18 19 and 21
Rolling rocket model	0.53 to 1.9	1,350,000 to 7,450,000		Three-finned RM-5 rocket	12	22

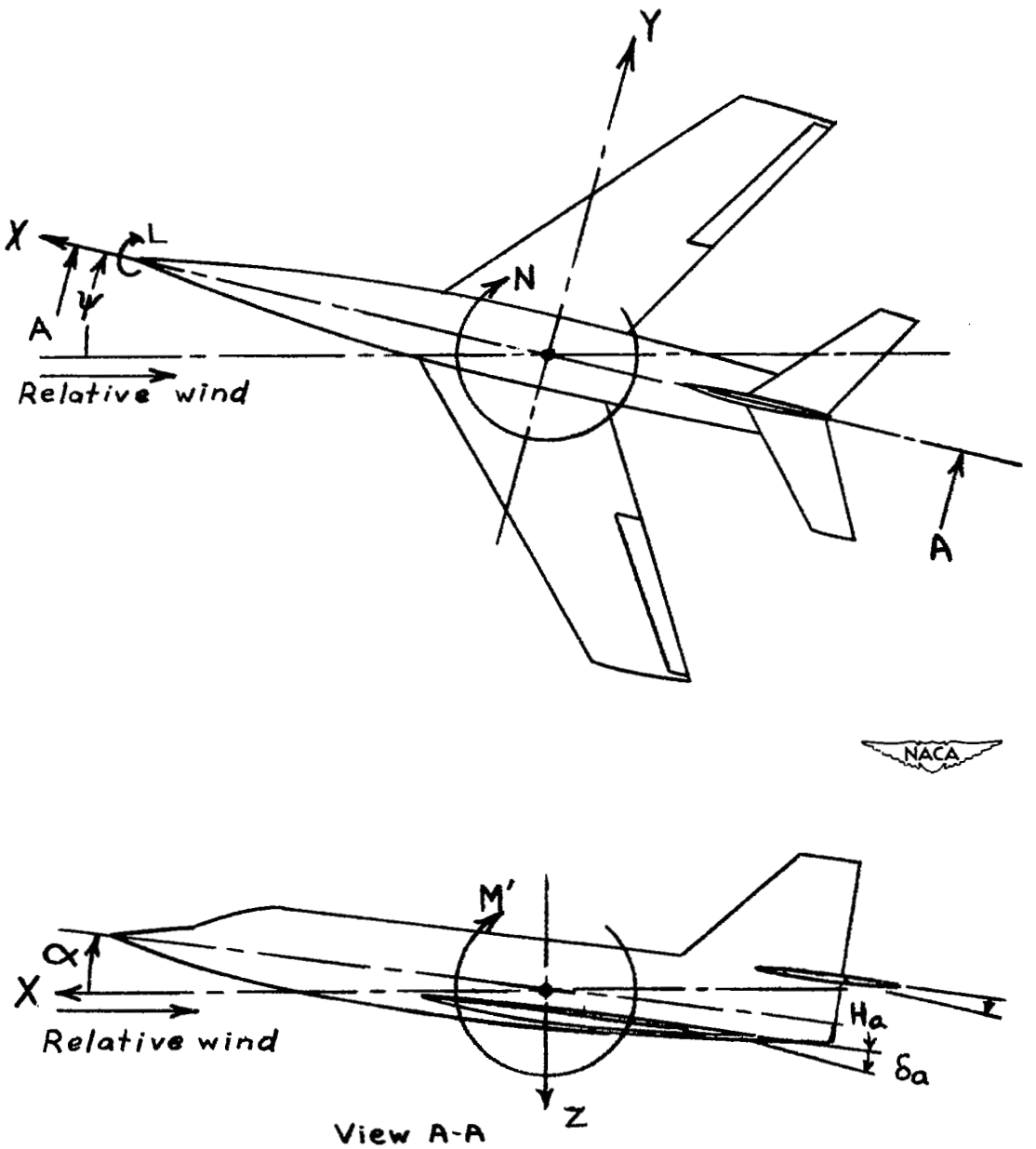

Figure 1.- System of stability axes. Arrows indicate positive values.

[redacted]

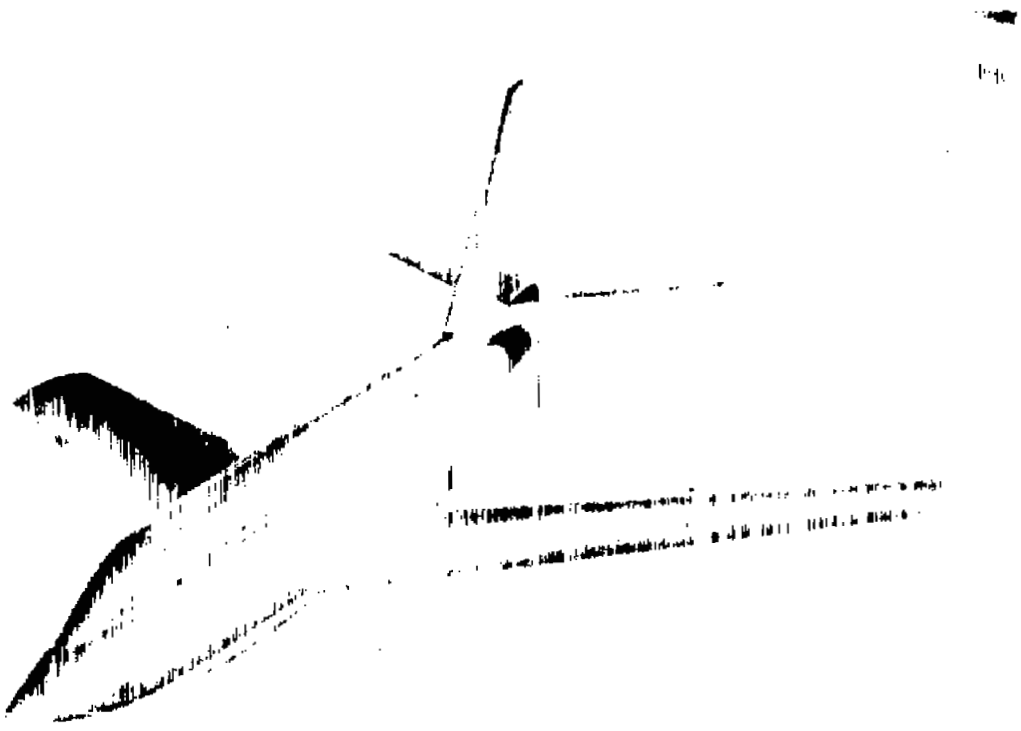

NACA
L-64078.1

Figure 2.- Basic model.

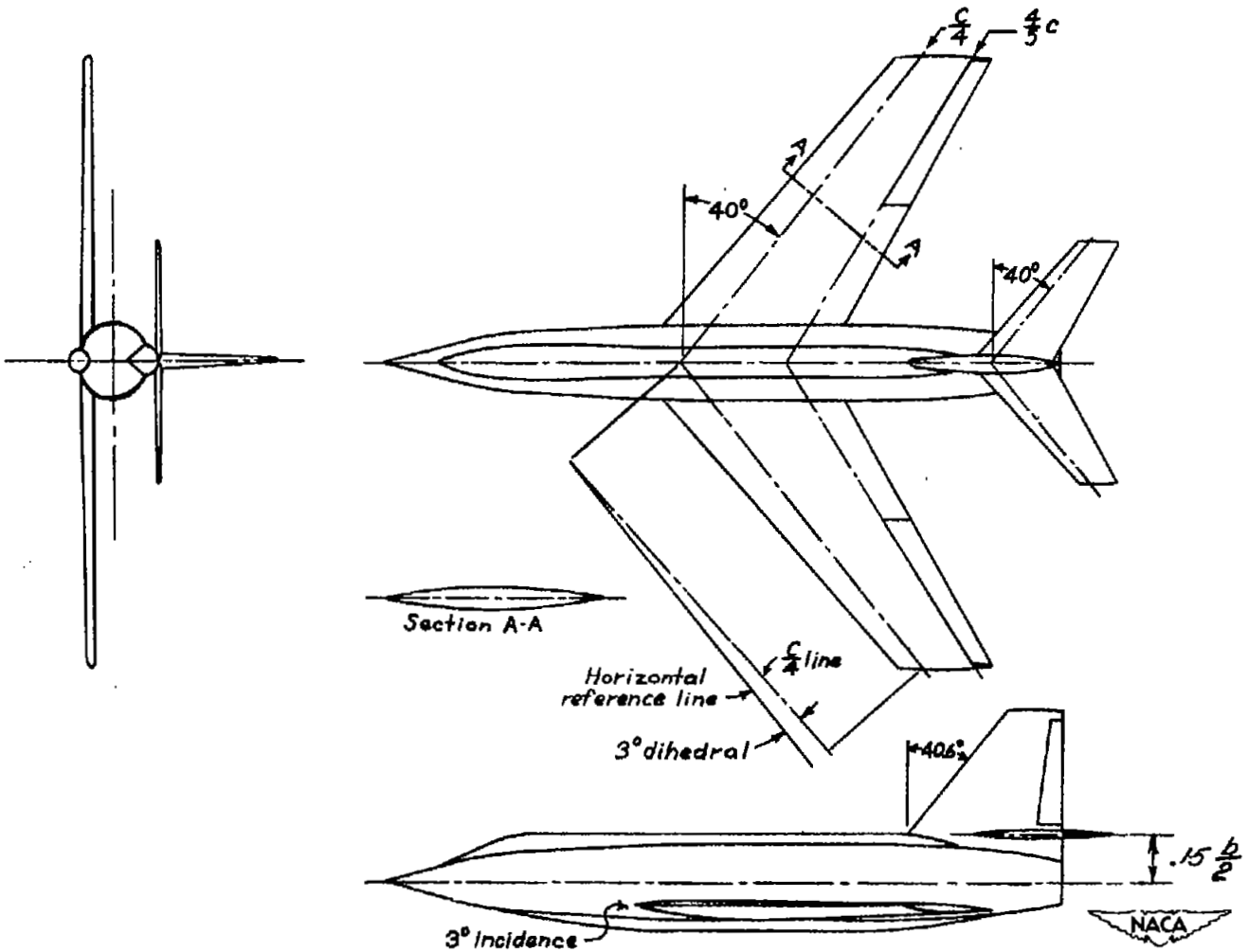

(a) Basic model.

Figure 3.- Details of models of supersonic aircraft configuration.

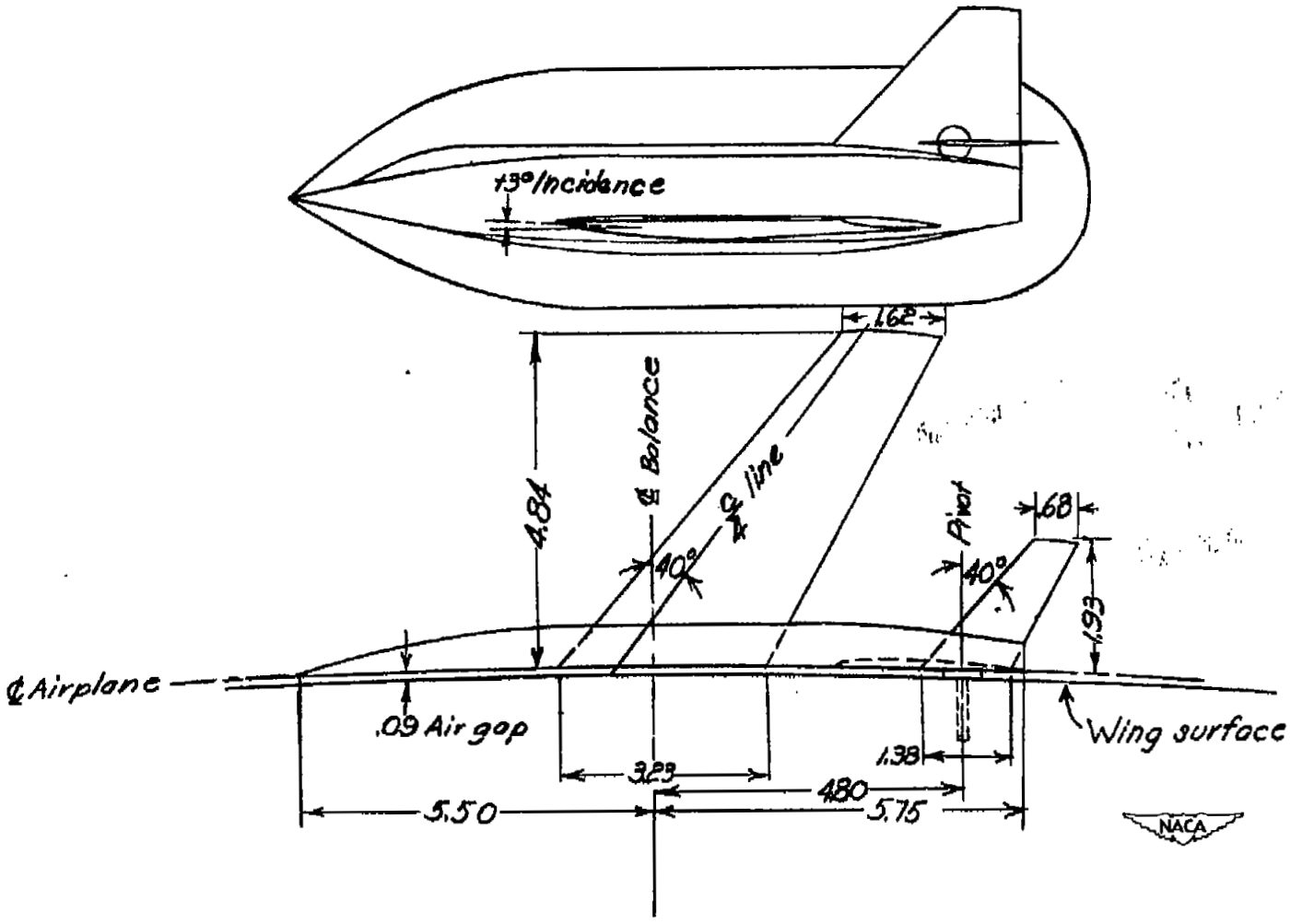

(b) Wing-flow model.

Figure 3.- Continued.

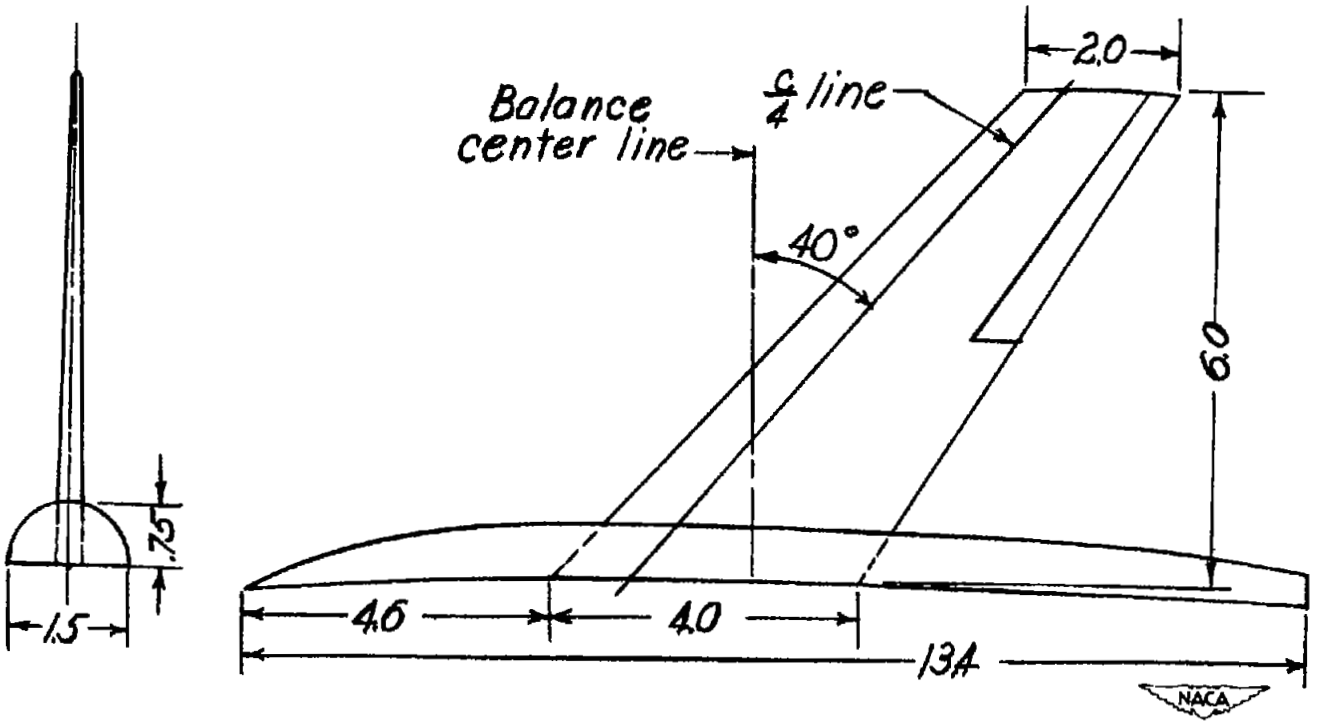

(c) Bump model.

Figure 3.- Continued.

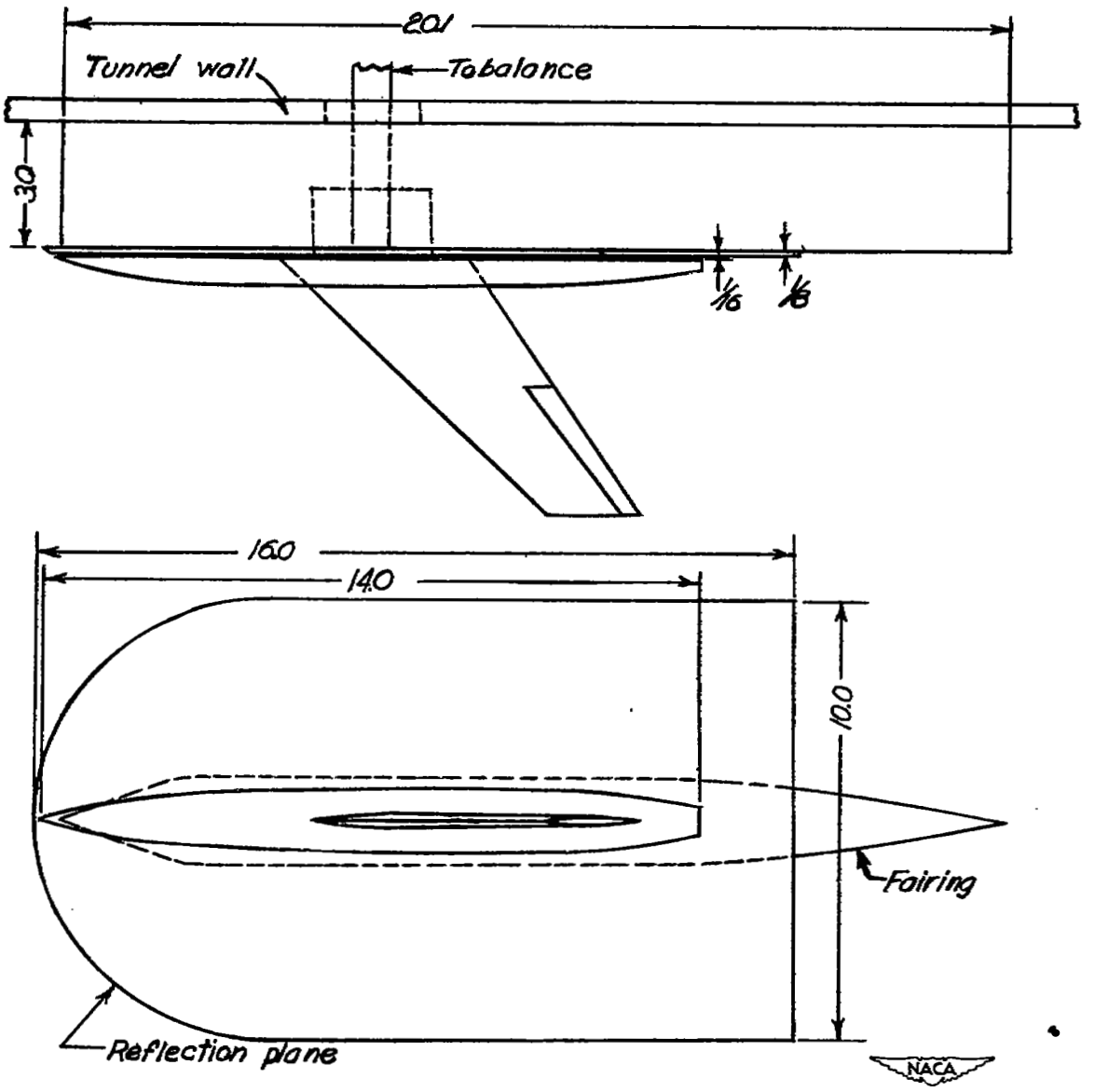

(d) Wall model.

Figure 3.- Continued.

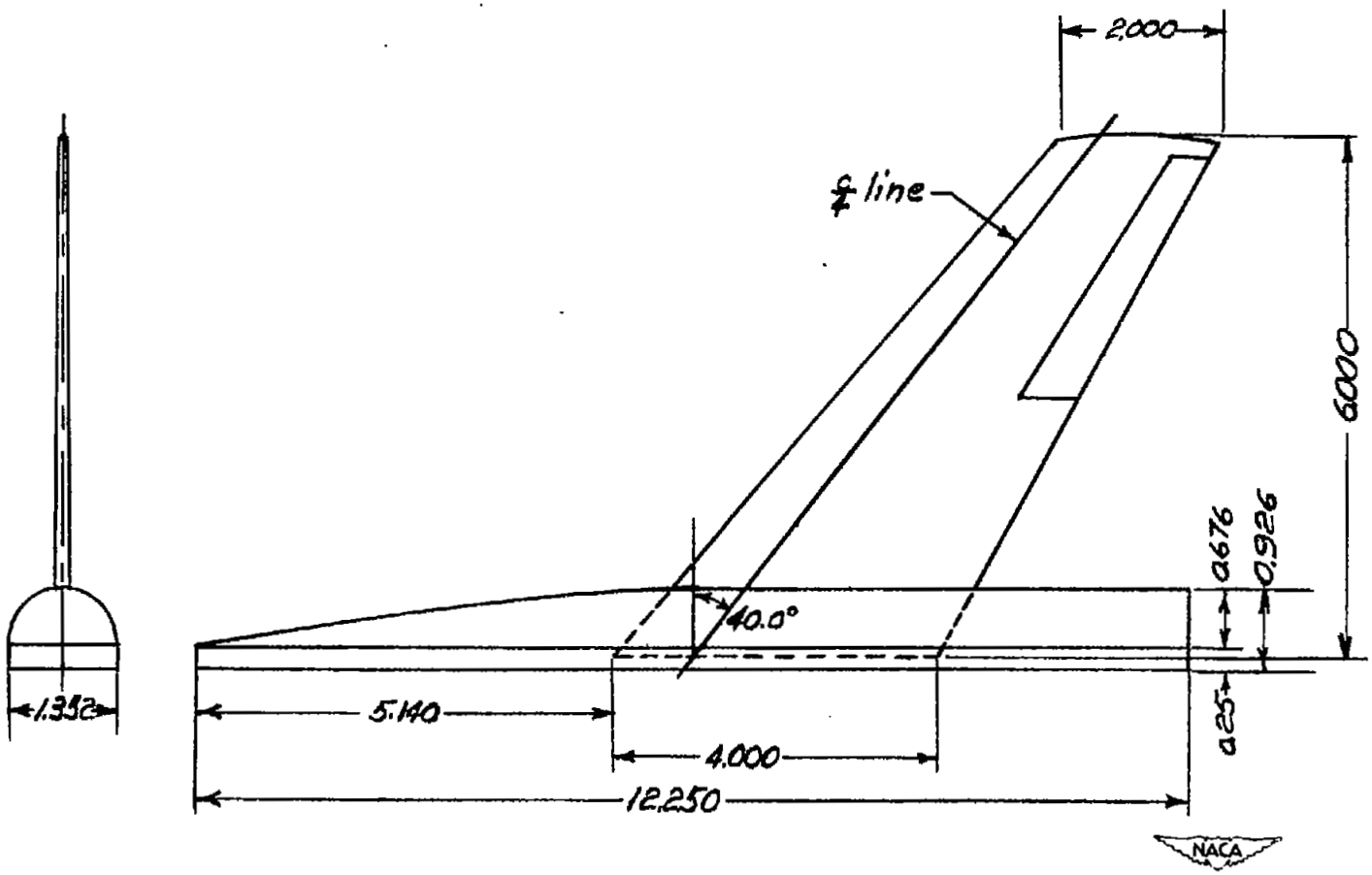

(e) Langley 9- by 12-inch supersonic blowdown tunnel model.

Figure 3.- Continued.

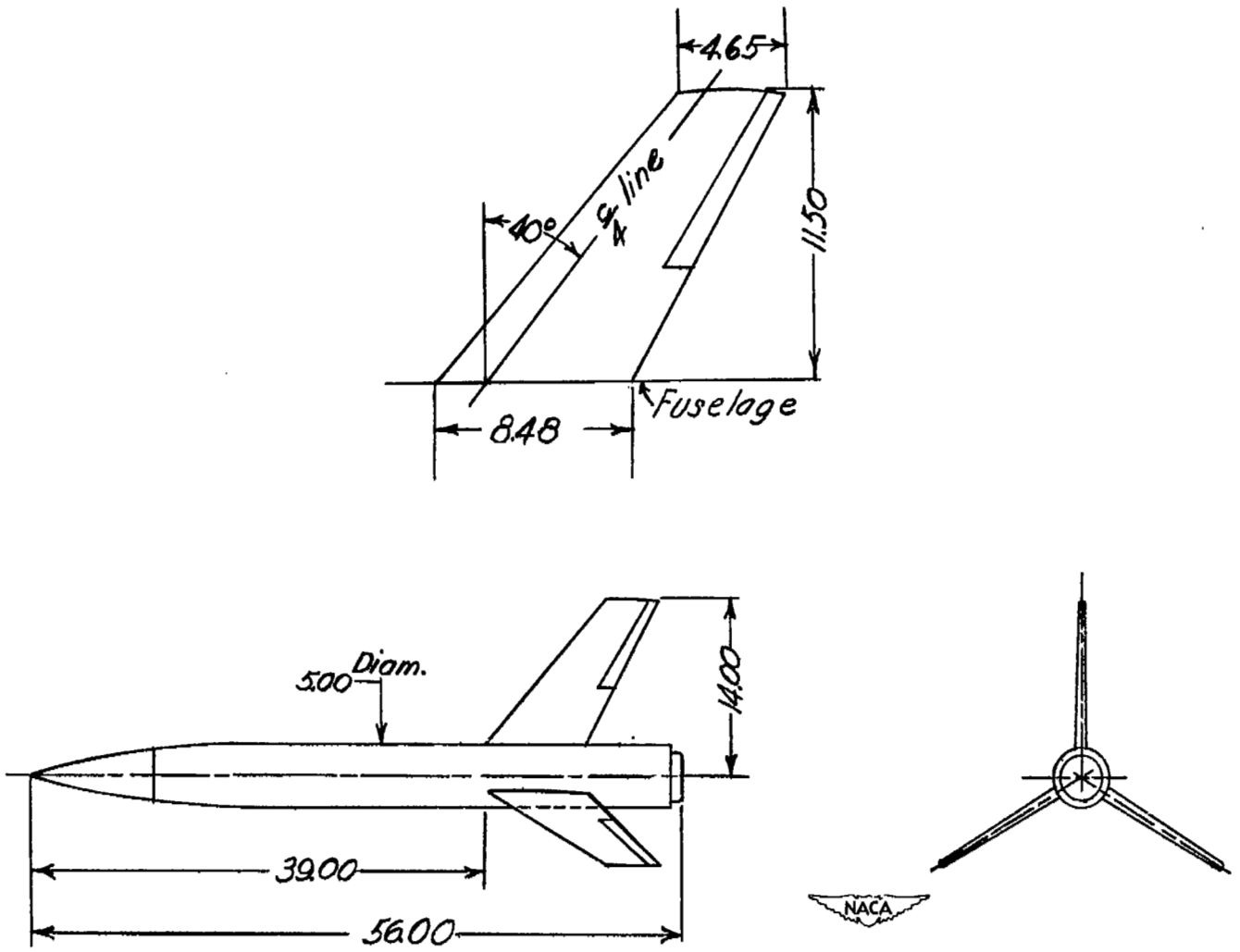

(f) RM-5 rocket model.

Figure 3.- Concluded.

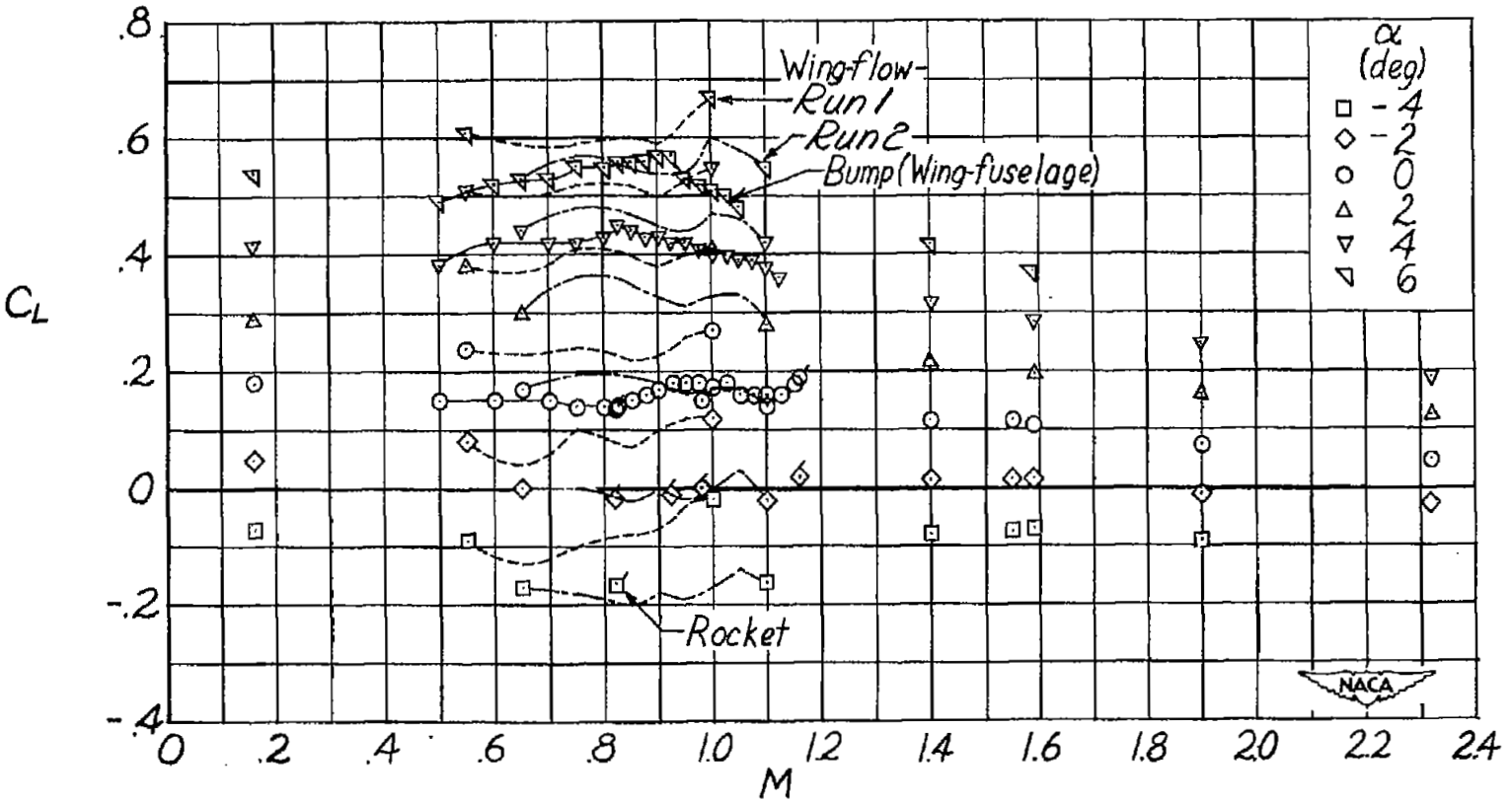

Figure 4.- Variation of lift coefficient with Mach number for several angles of attack as obtained from various sources.

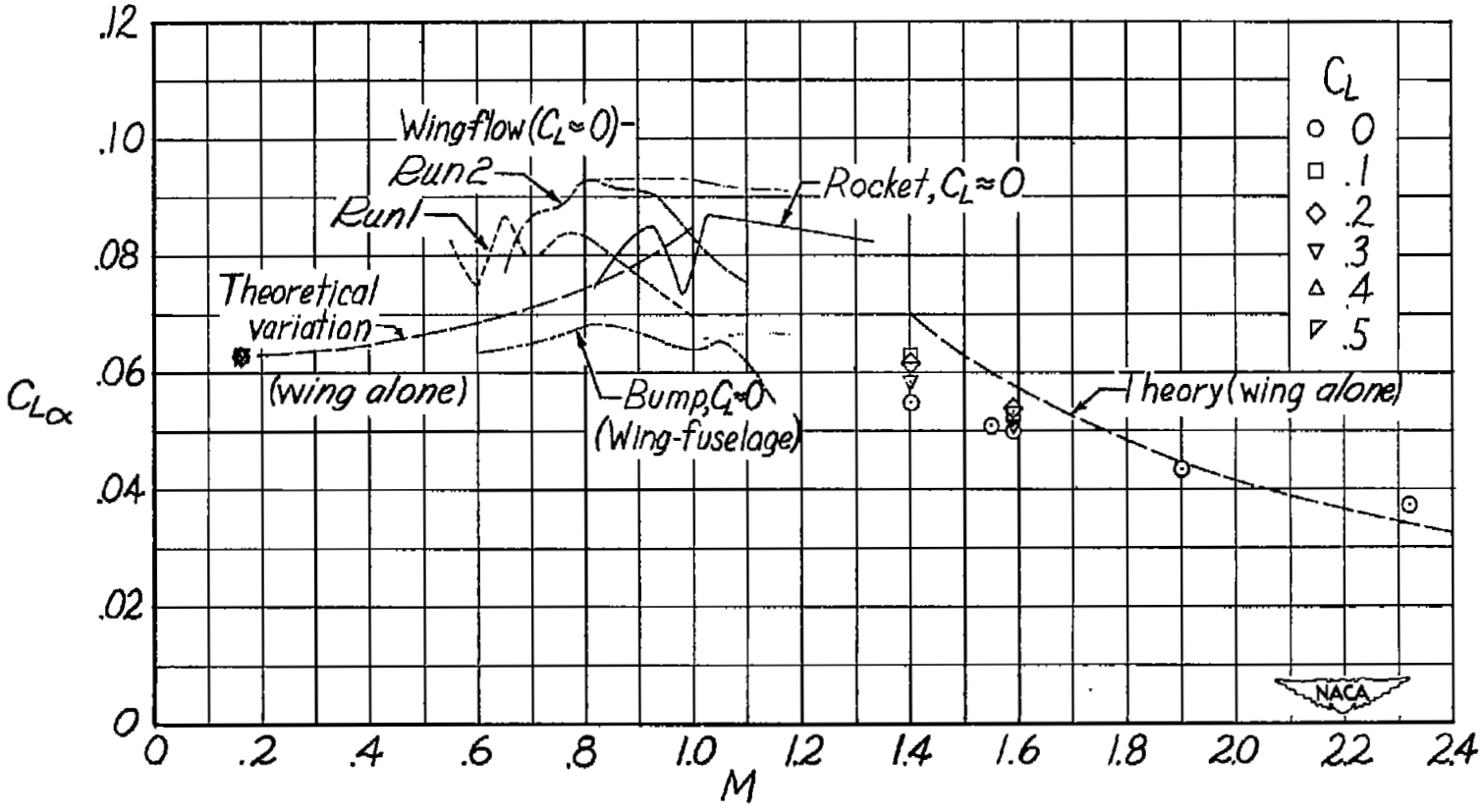

Figure 5.- Variation of lift-curve slope with Mach number for several lift coefficients. Complete model.

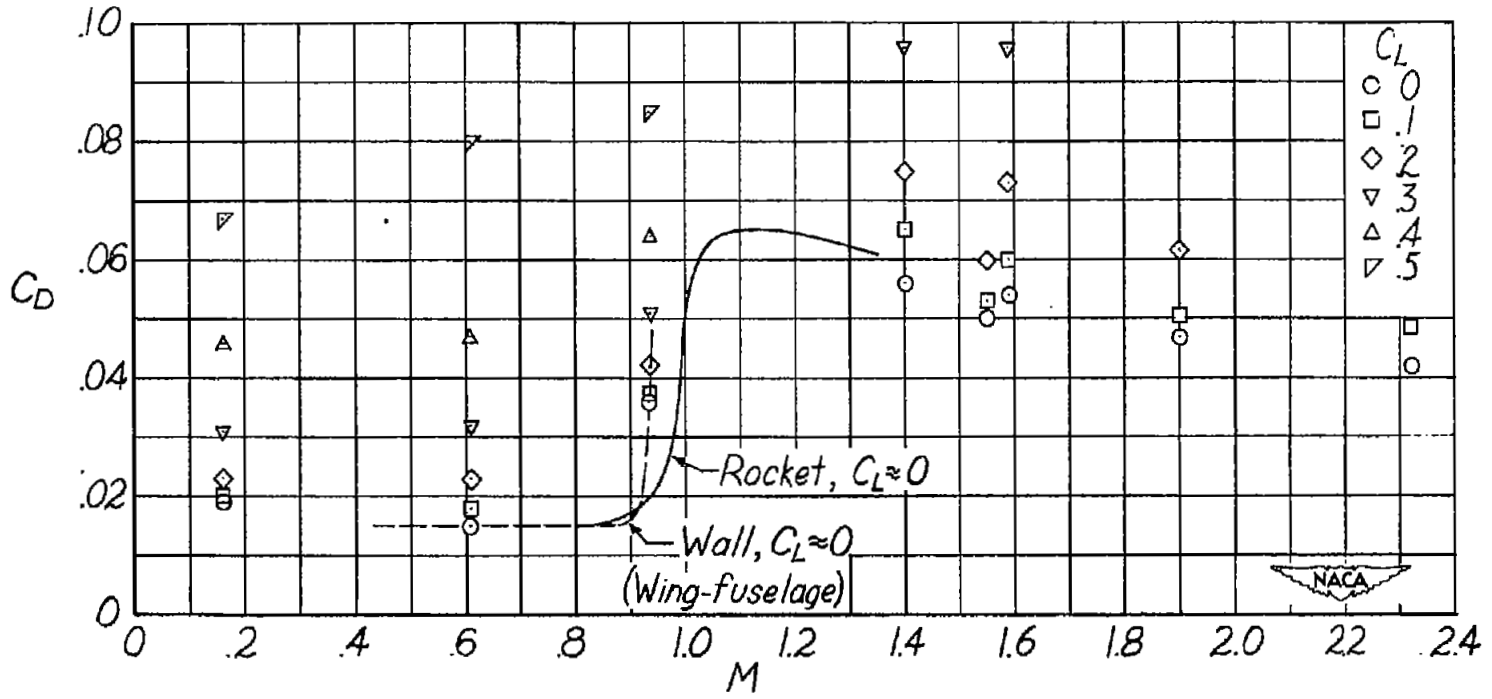

Figure 6.- Variation of drag coefficient with Mach number for several lift coefficients as obtained from various sources.

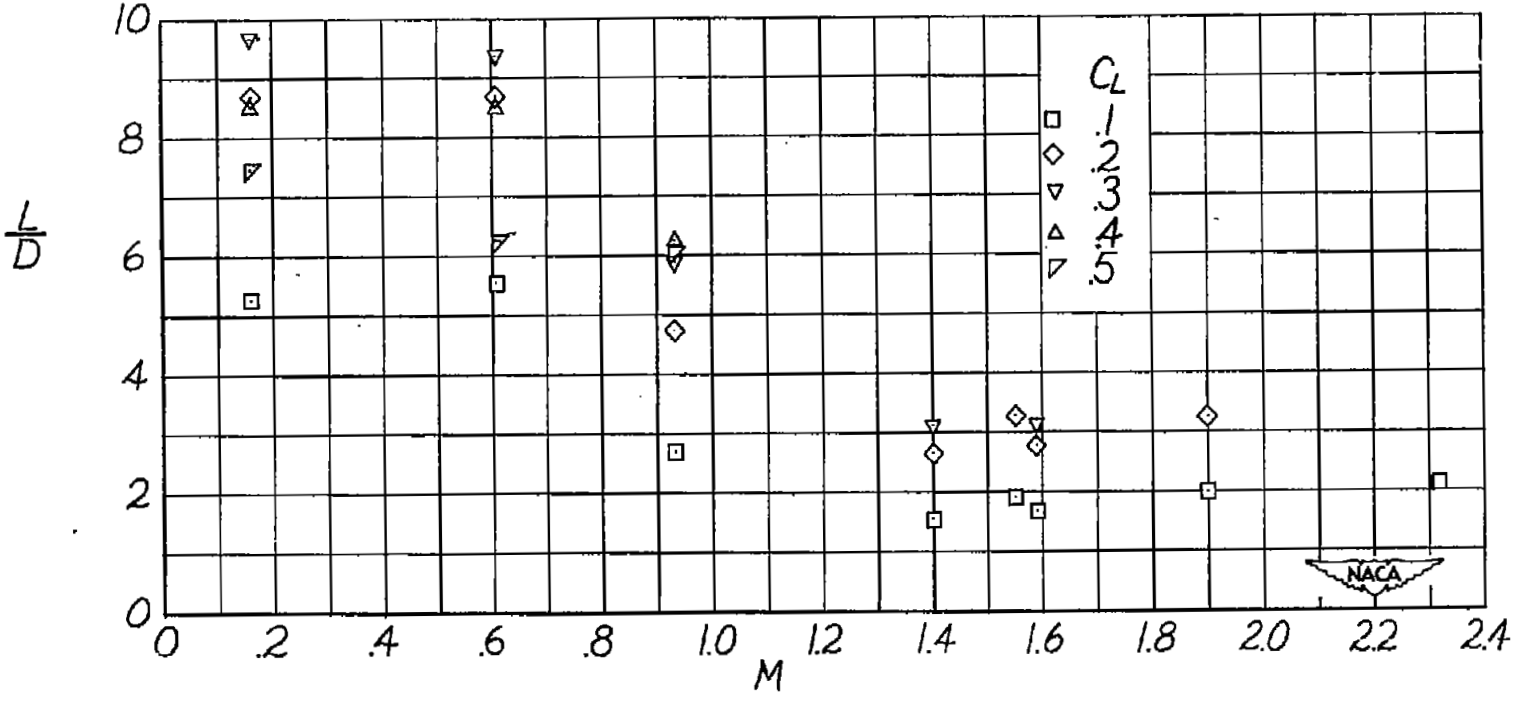

Figure 7.- Variation of lift-drag ratio with Mach number for several lift coefficients.

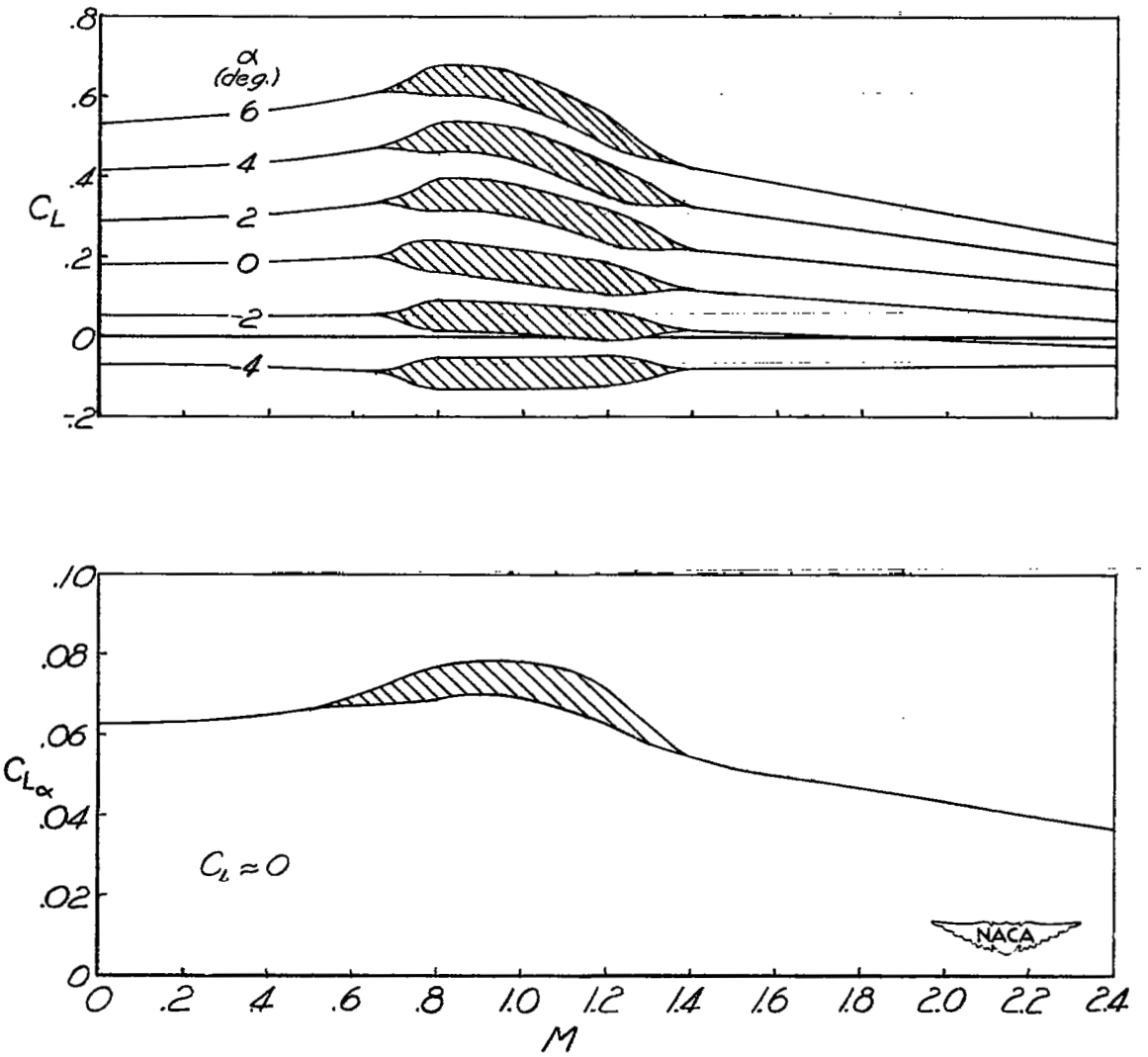

Figure 8.- Variation of lift and drag characteristics with Mach number.

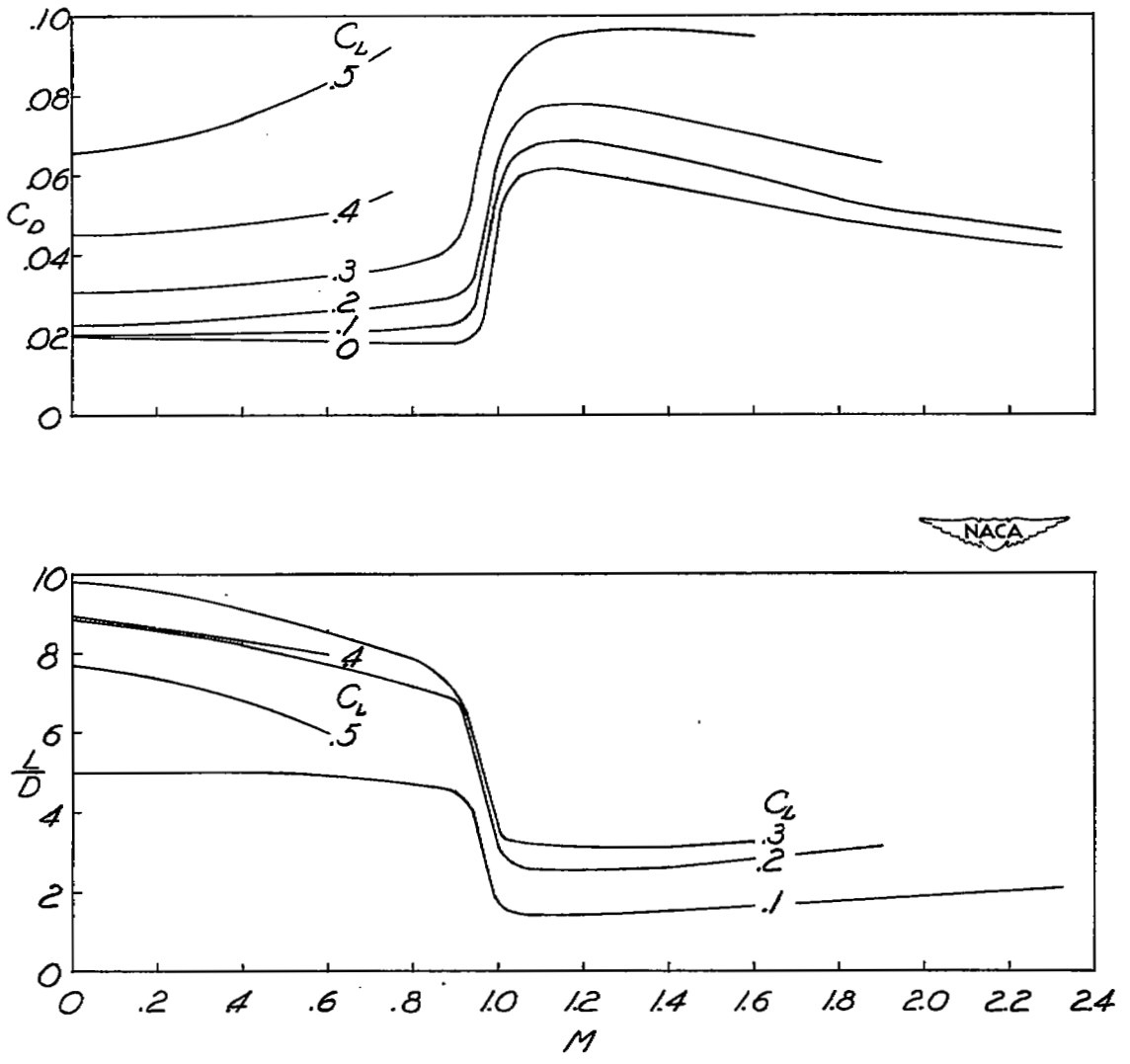

Figure 8.- Concluded.

[redacted]

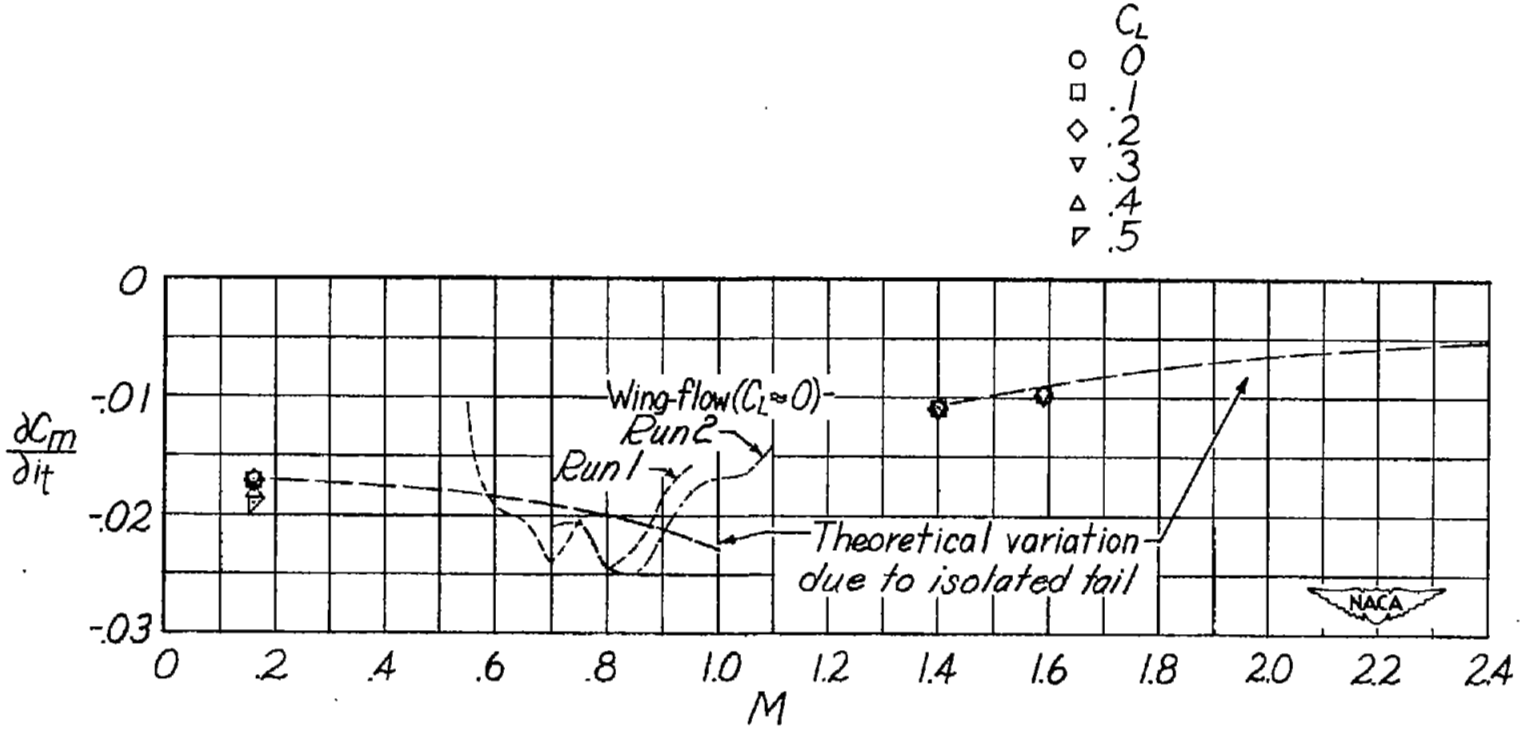

Figure 9.- Variation of stabilizer effectiveness with Mach number as obtained from various sources.

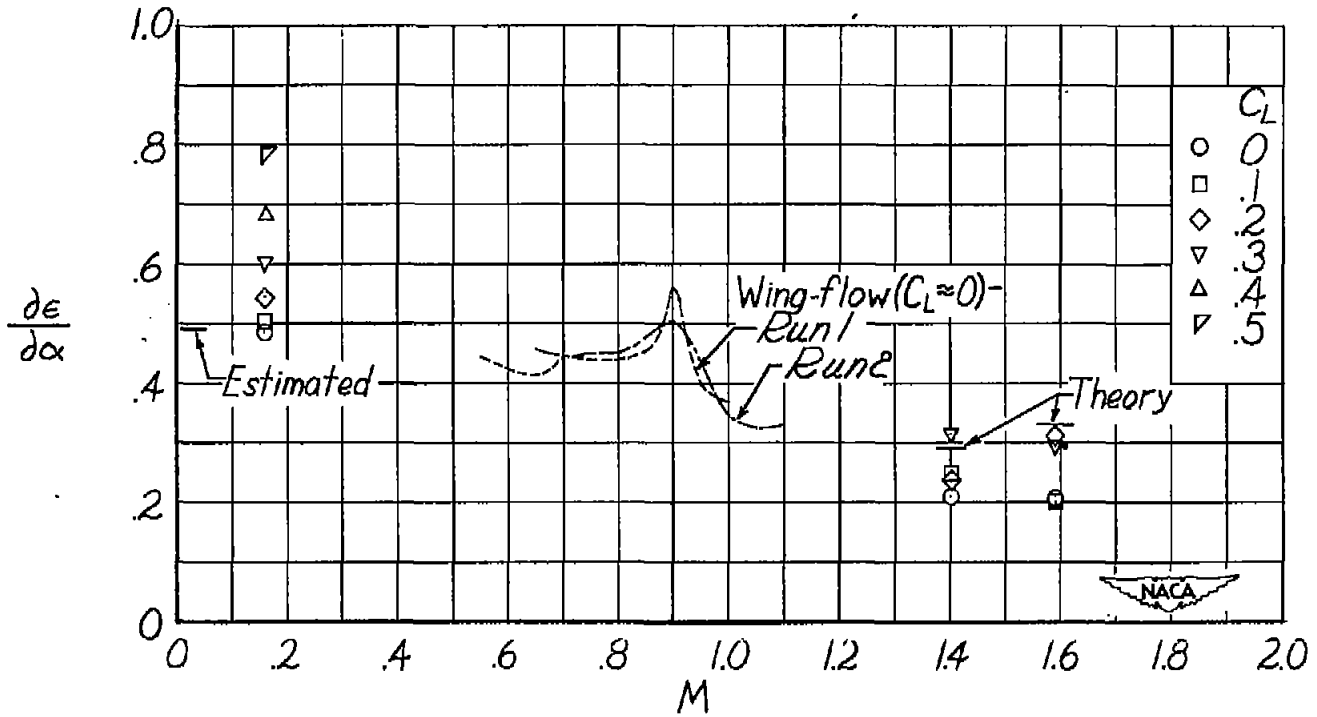

Figure 10.- Variation of the downwash factor $\partial\epsilon/\partial\alpha$ with Mach number as obtained from various sources.

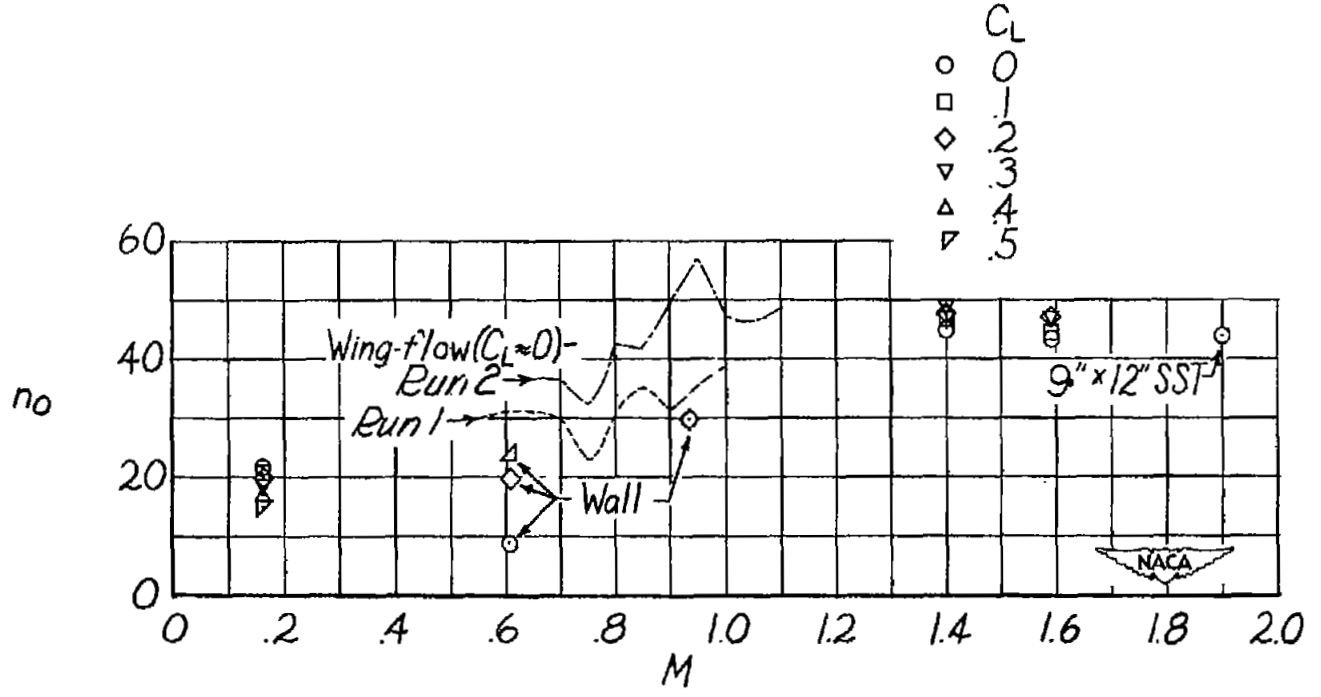

Figure 11.- Variation of the tail-off aerodynamic-center location with Mach number as obtained from various sources.

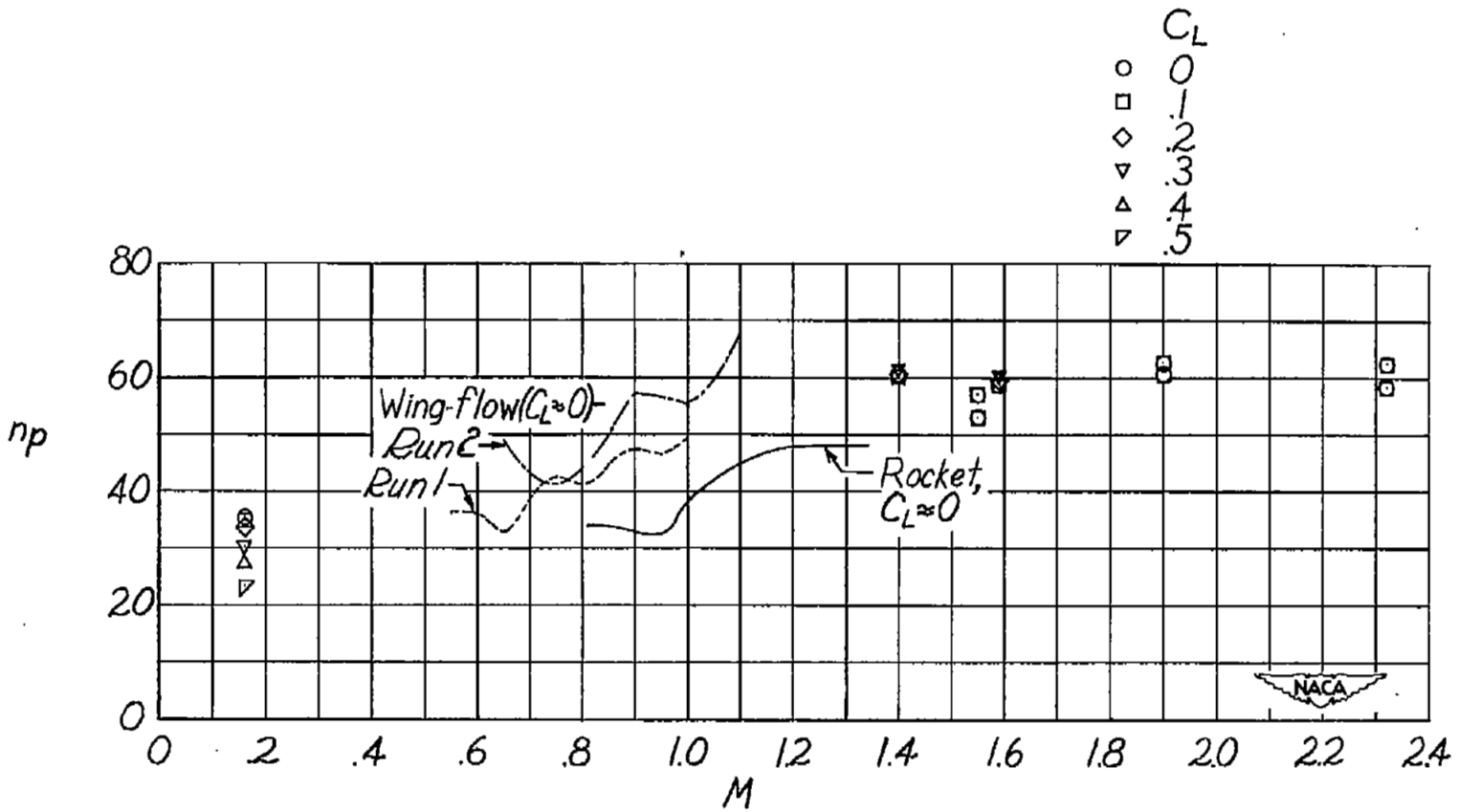

Figure 12.- Variation of the neutral-point location with Mach number as obtained from various sources.

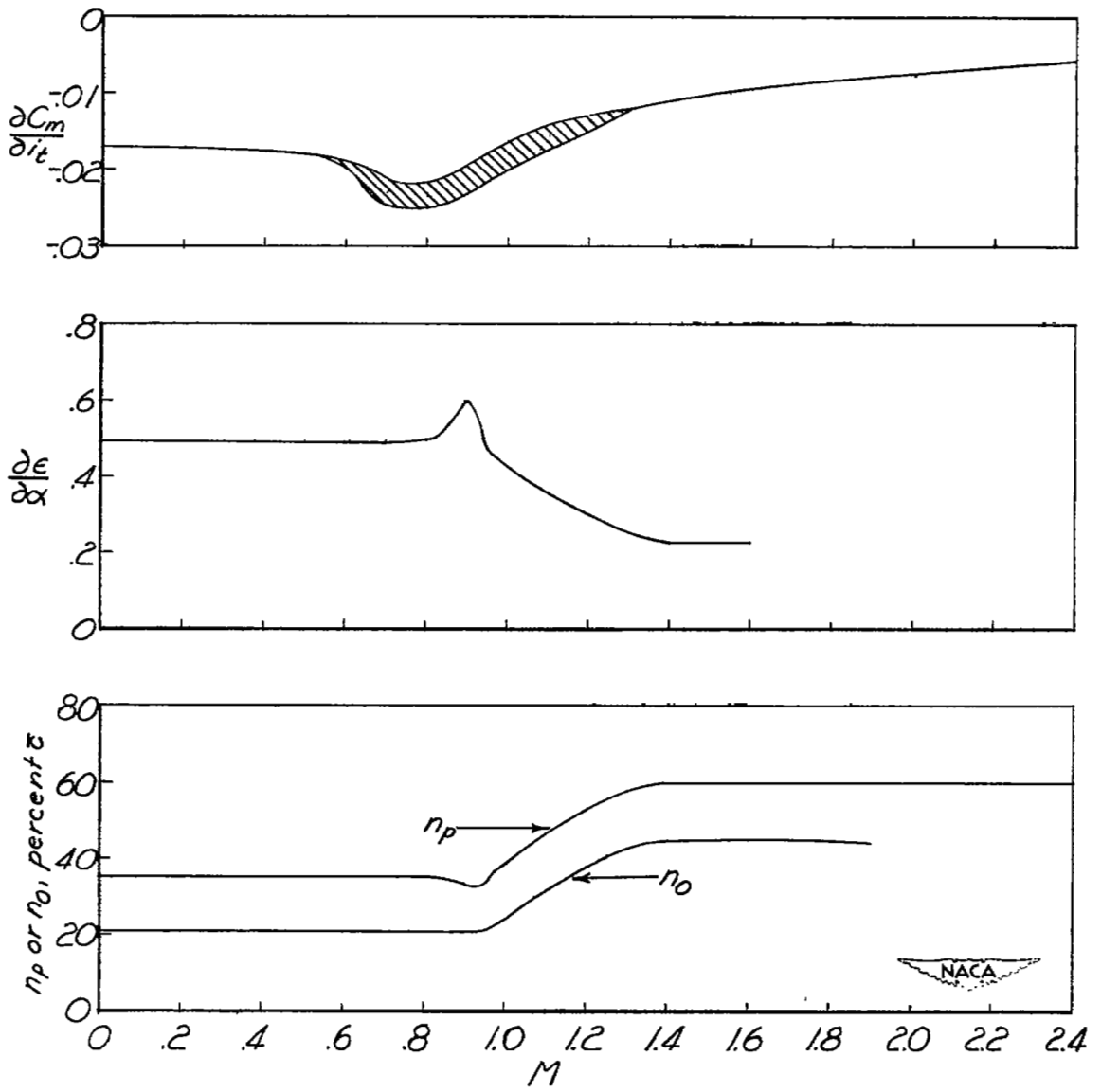

Figure 13.- Variation of longitudinal stability characteristics with Mach number. $C_L \approx 0$.

[redacted]

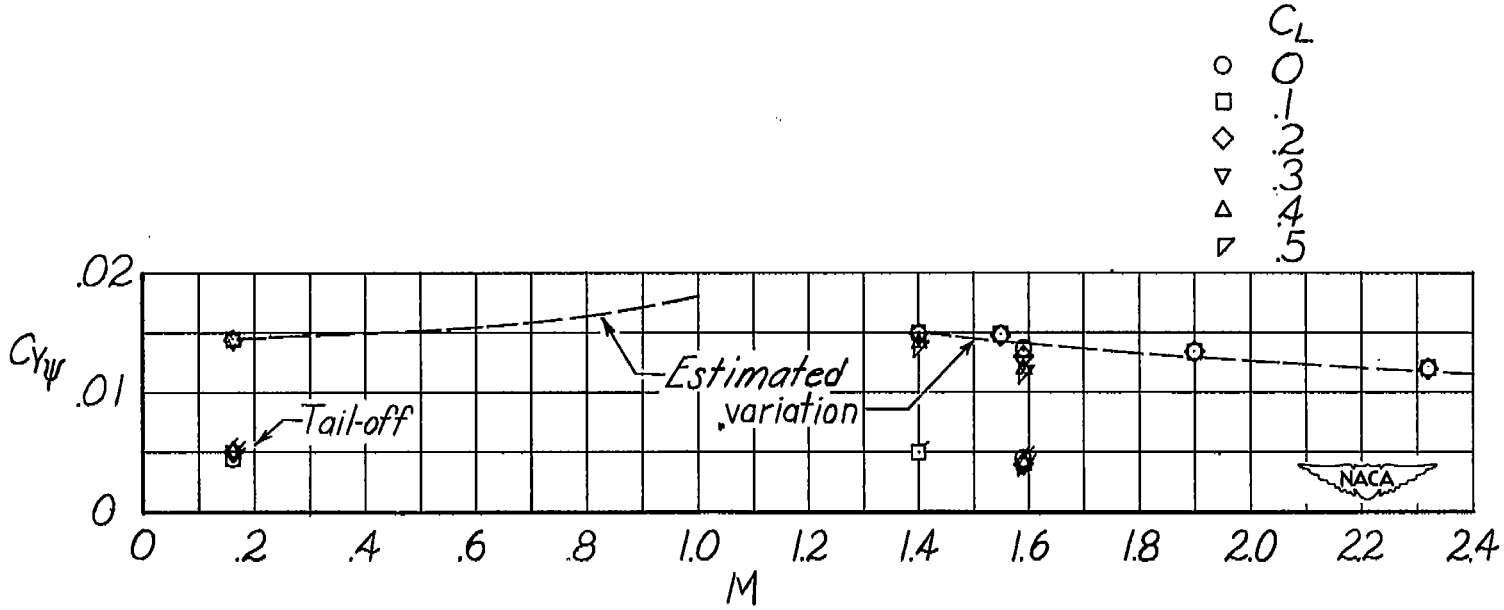

Figure 14.- Variation of the static lateral-force derivative with Mach number.

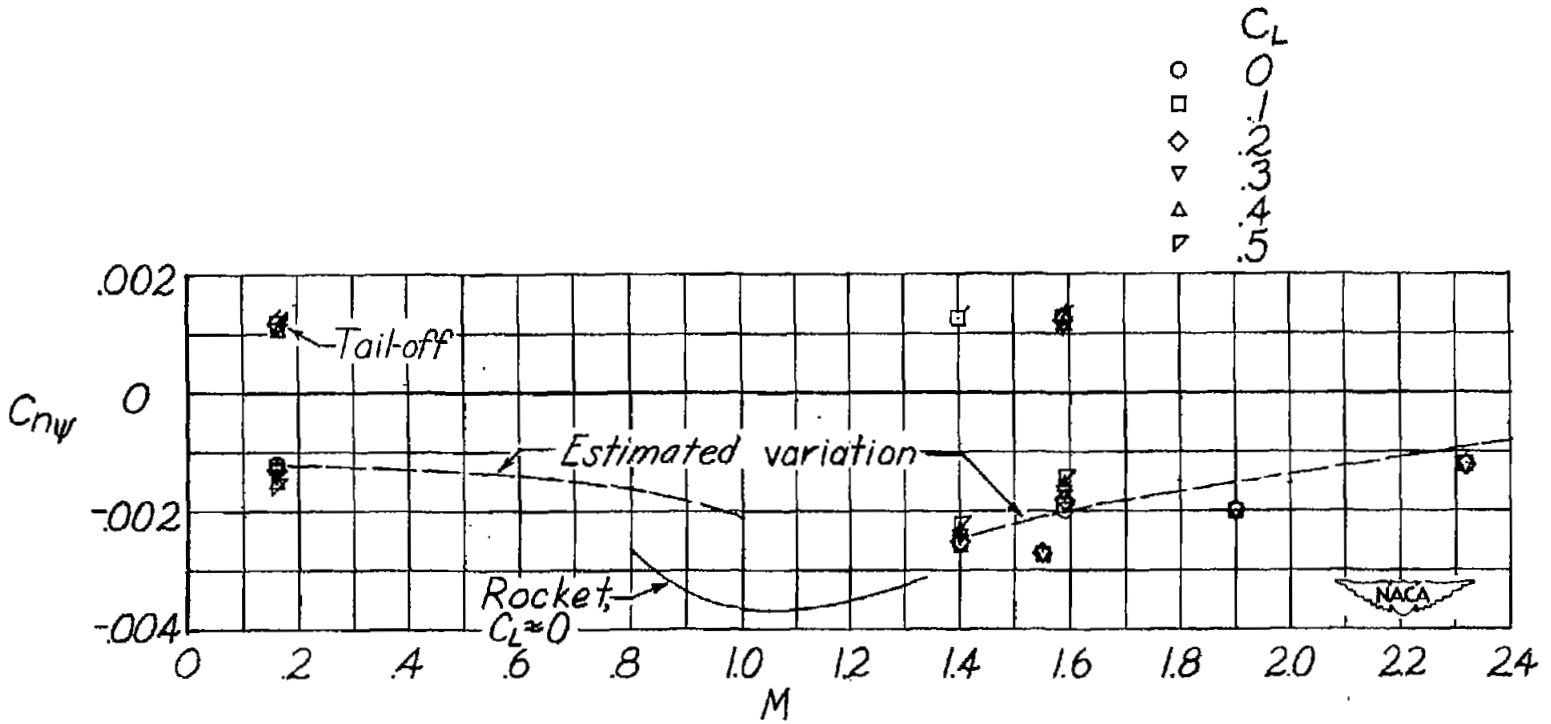

Figure 15.- Variation of the directional stability derivative with Mach number.

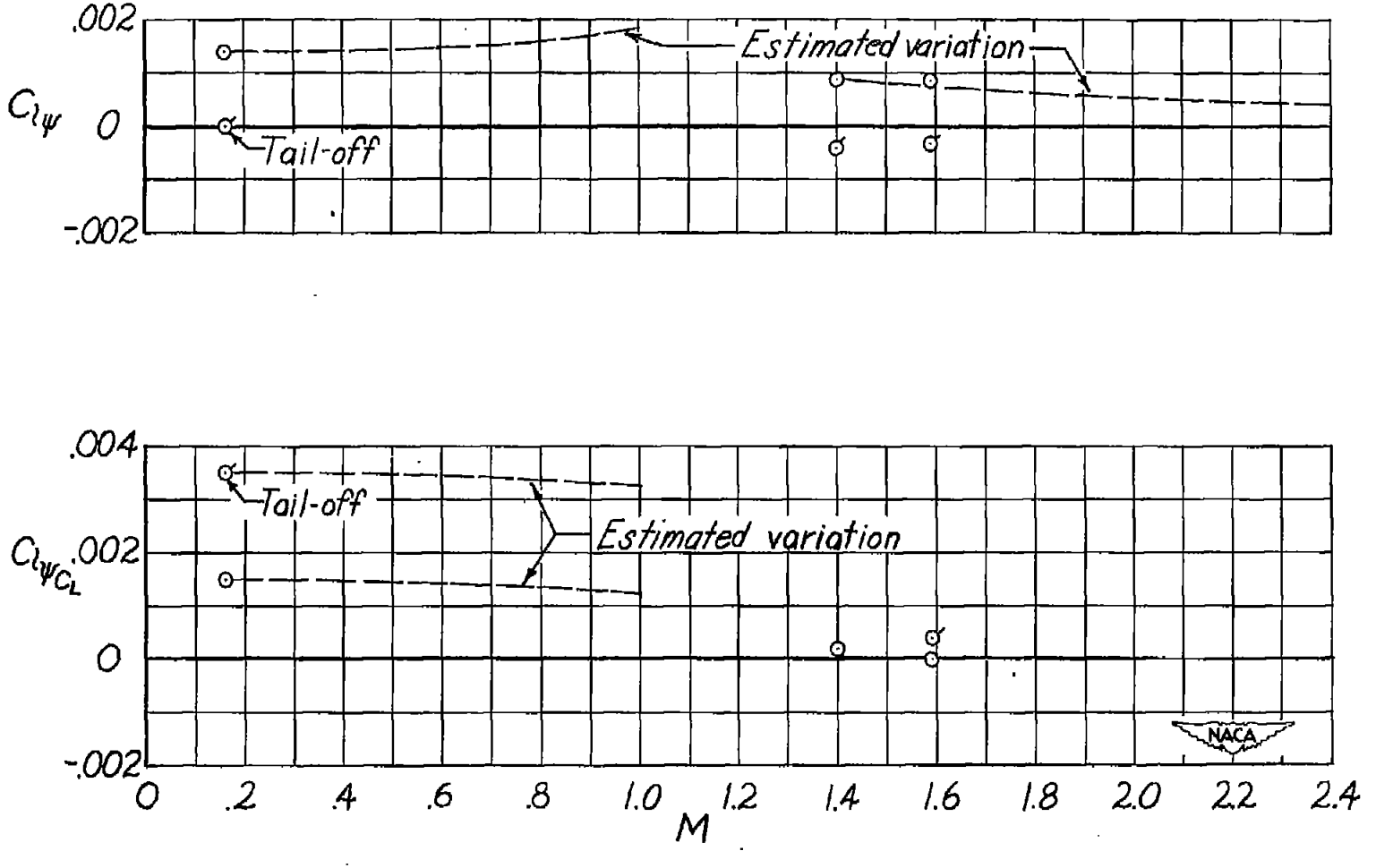

Figure 16.- Variation of effective dihedral derivatives with Mach number. $C_L \approx 0$.

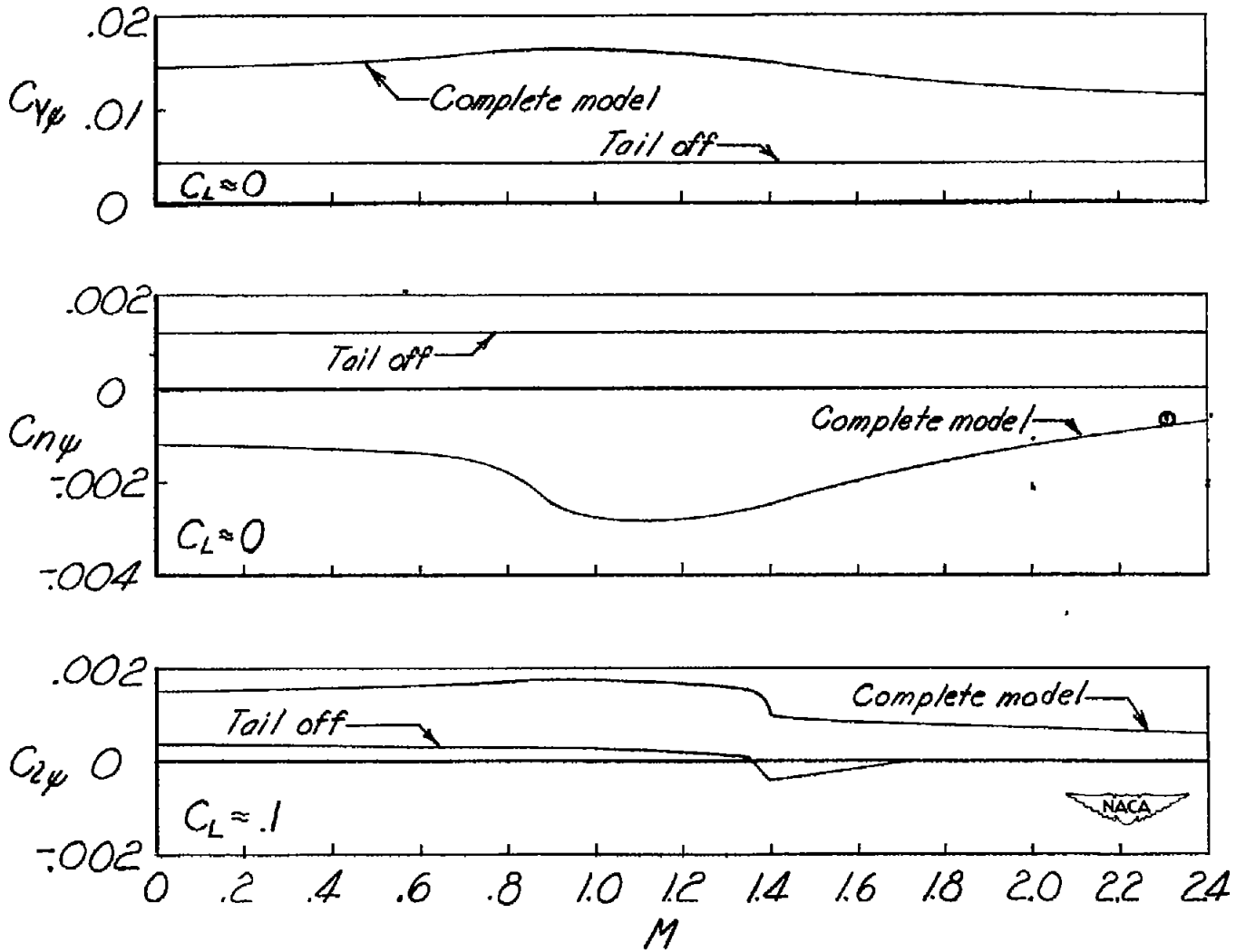

Figure 17.- Variation of the sideslip derivatives with Mach number.

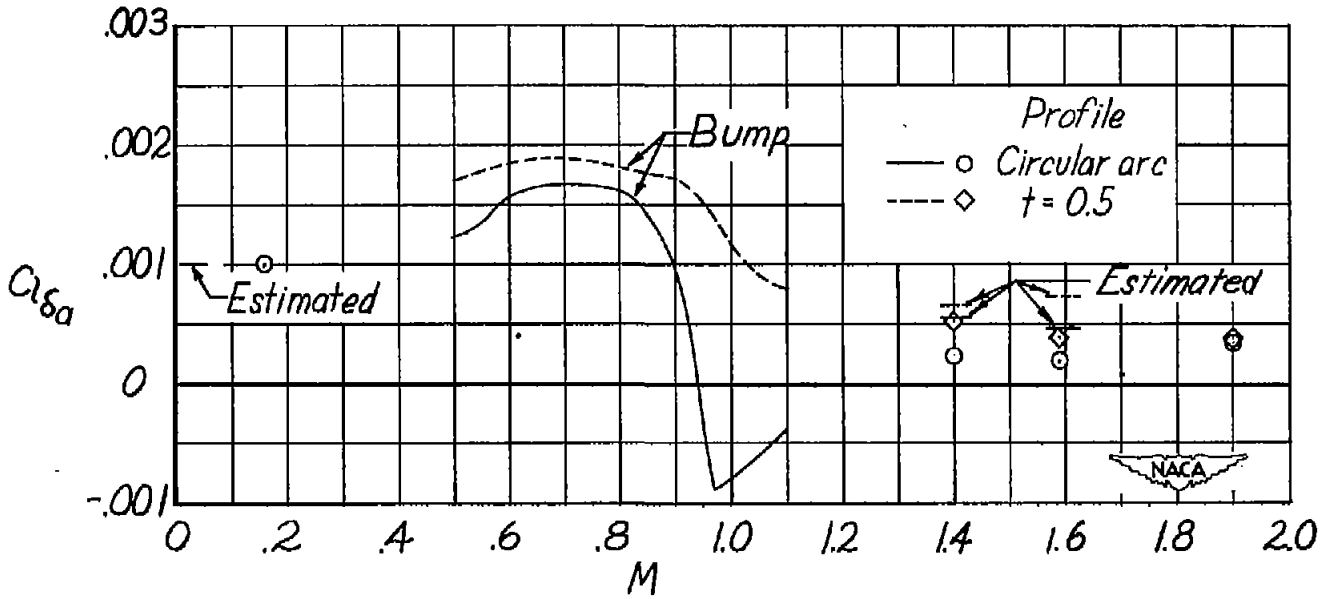

Figure 18.- Variation of aileron effectiveness derivative with Mach number. C_L, $\delta_a \approx 0$.

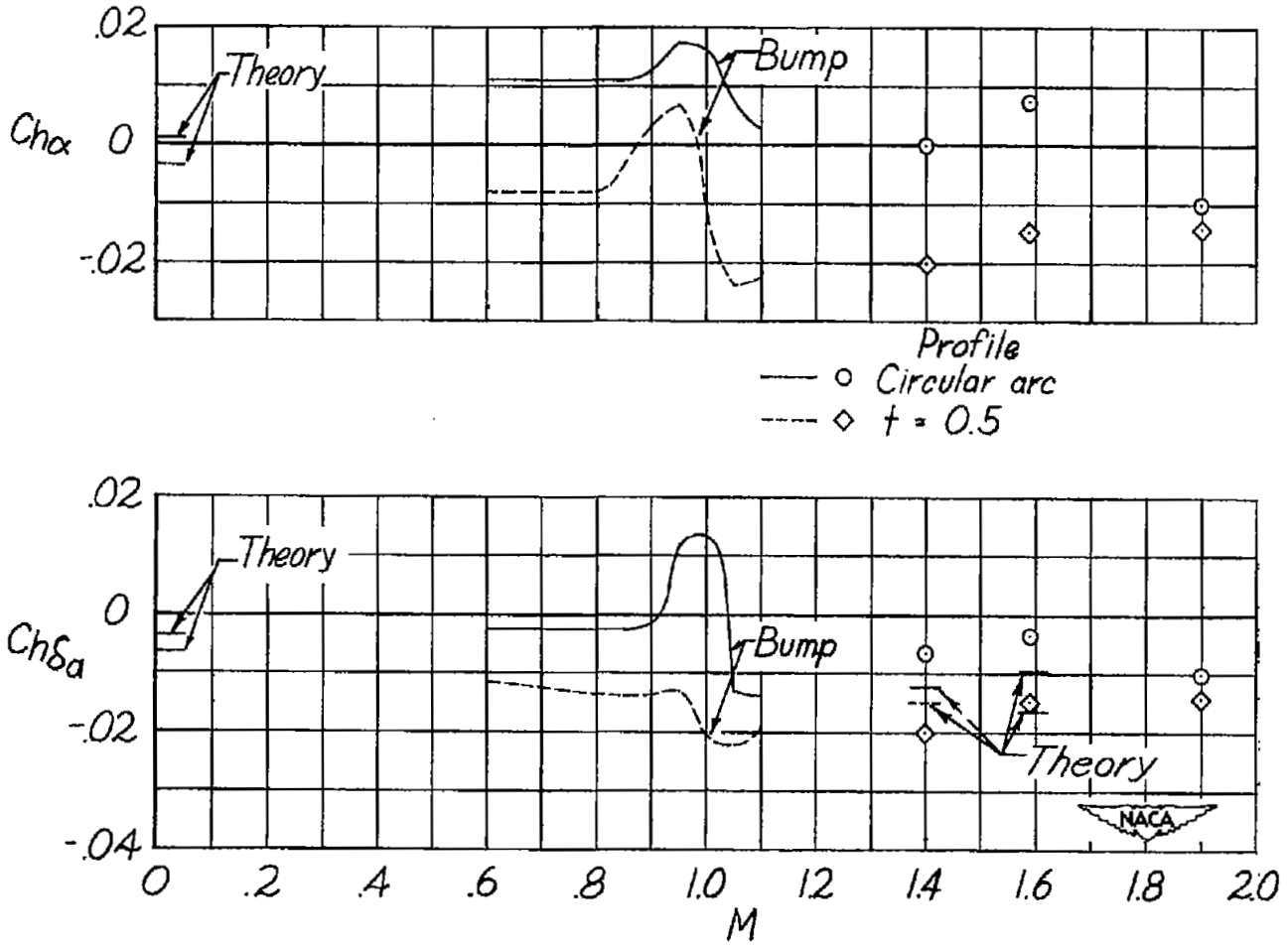

Figure 19.- Variation of aileron hinge-moment characteristics with Mach number. C_L, $\delta_a \approx 0$.

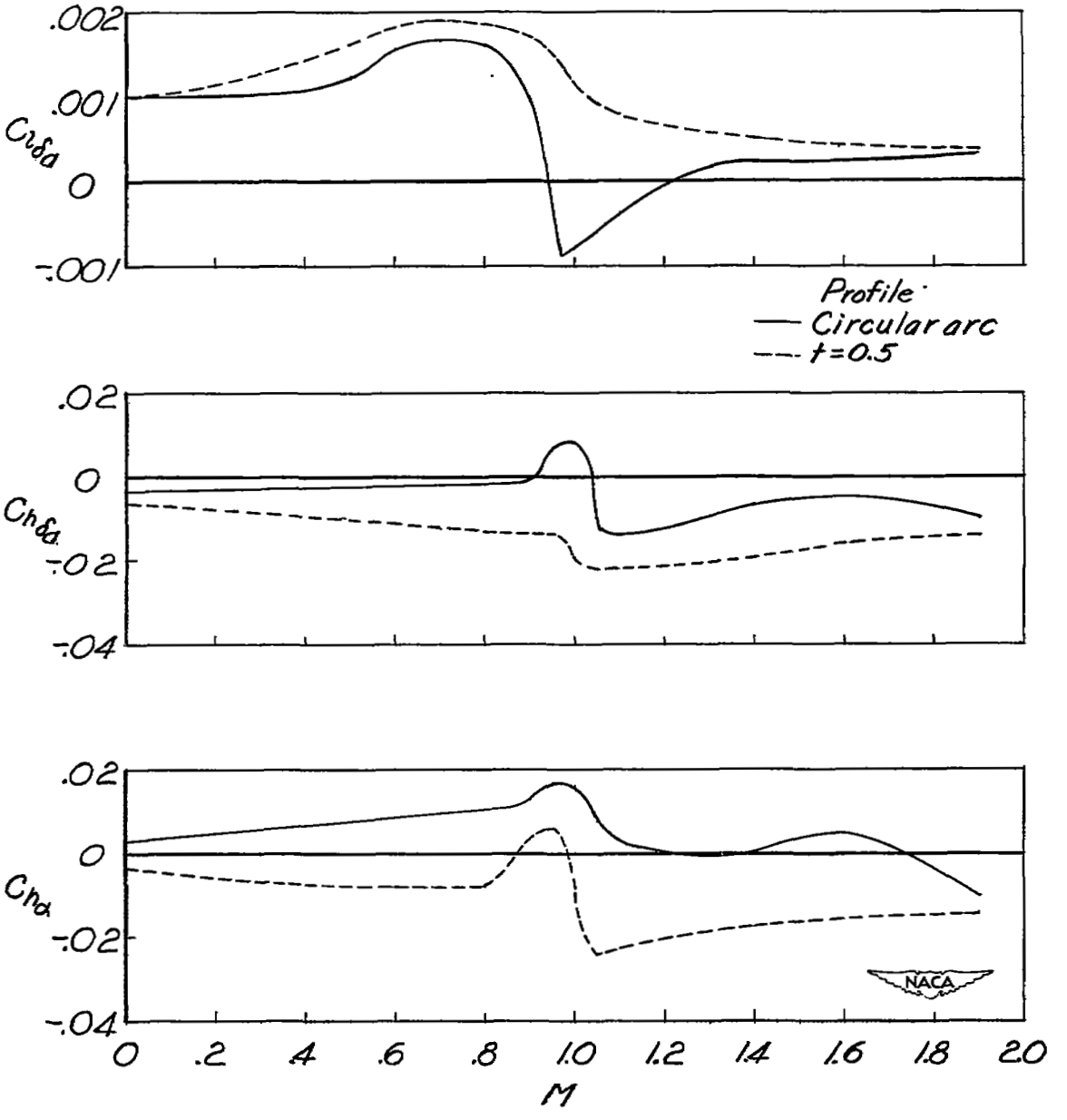

Figure 20.- Variation of aileron characteristics with Mach number. C_L, $\delta_a \approx 0$.

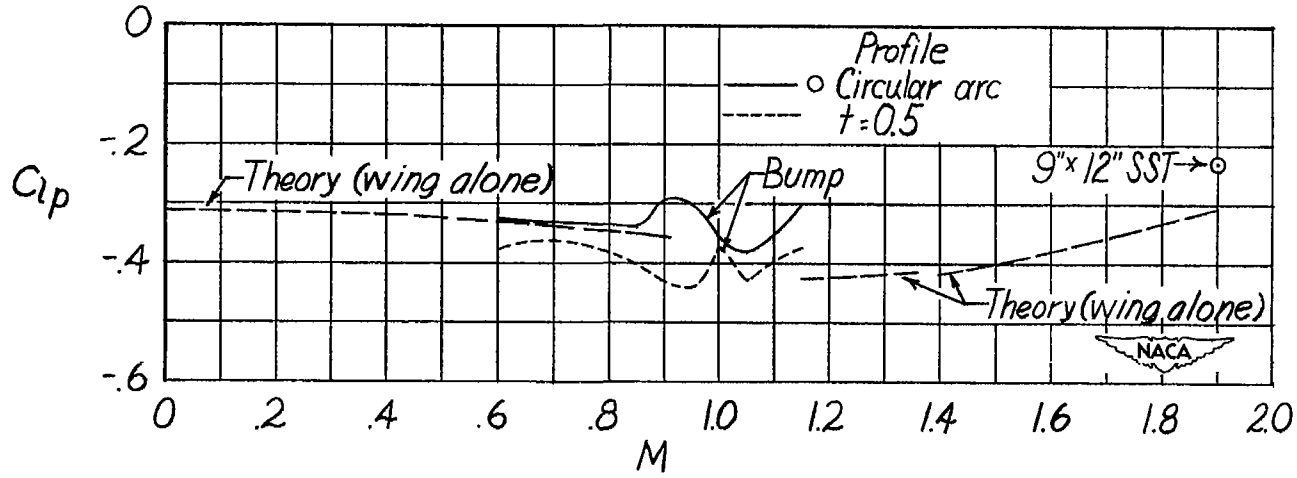

Figure 21.- Variation of the damping-in-roll factor C_{l_p} with Mach number.

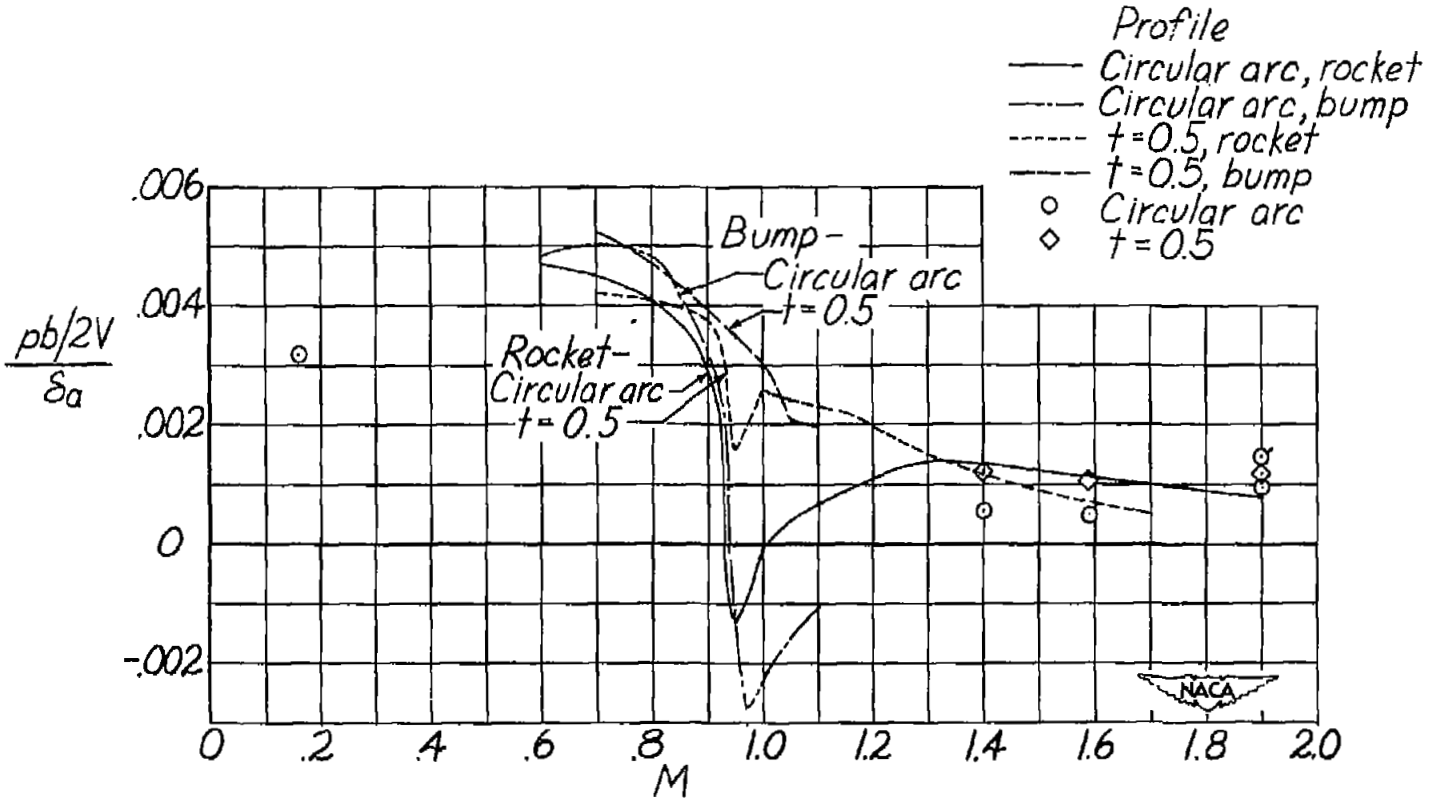

Figure 22.- Variation of rolling effectiveness with Mach number, C_L, $\delta_a \approx 0$. Flagged symbols (M = 1.90) from experimental $C_{l_{\delta_a}}$ and C_{l_p}; all others from experimental $C_{l_{\delta_a}}$ and theoretical C_{l_p}.

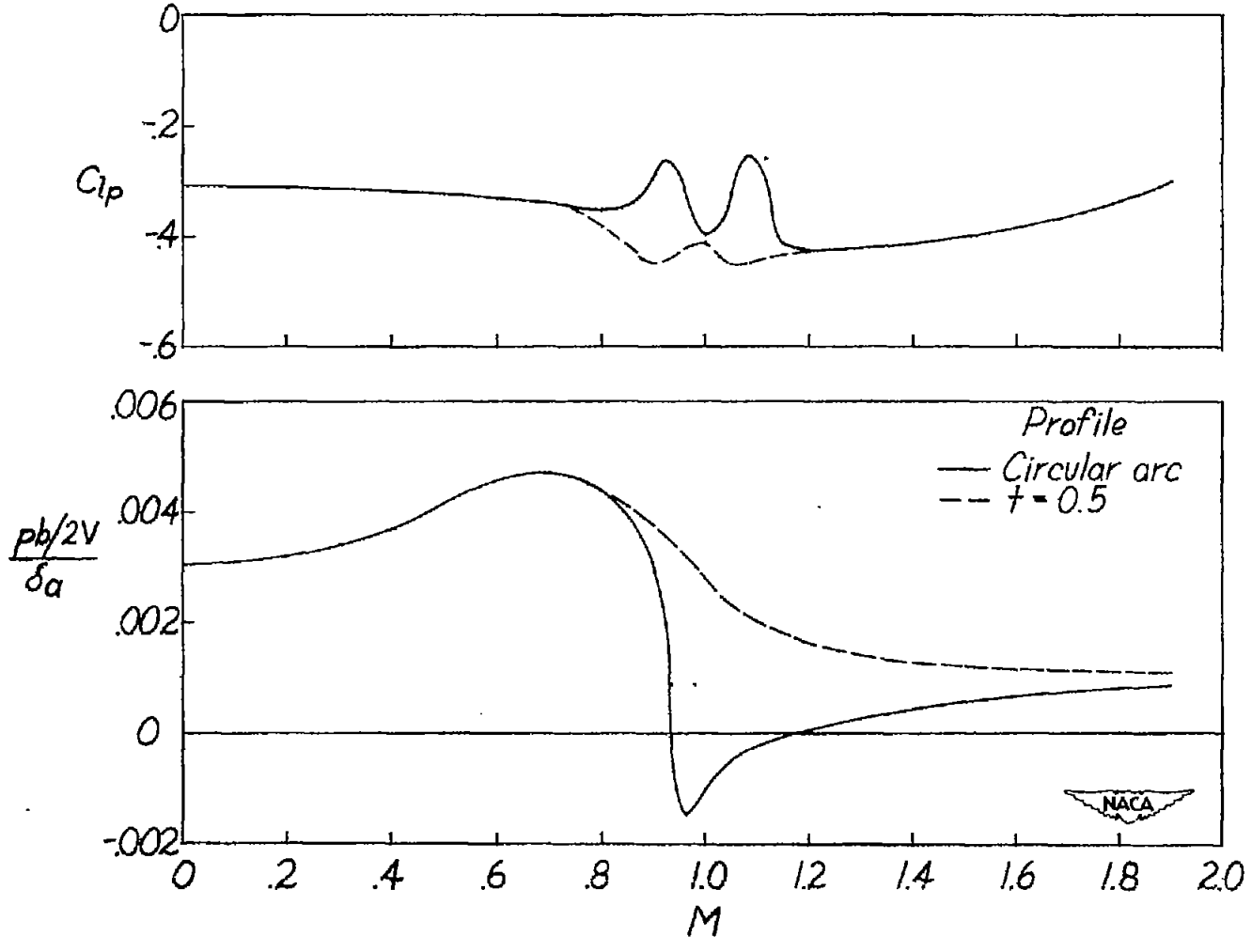

Figure 23.- Variation of damping-in-roll and rolling effectiveness with Mach number. C_L, $\delta_a \approx 0$.

NACA-Langley - 4-11-52 - 950

SECURITY INFORMATION

[redacted]

NASA Technical Library
3 1176 01437 0622

[redacted]